Hybrid Well-balanced WENO Schemes with Different Indicators for Shallow Water Equations

Gang Li, Changna Lu & Jianxian Qiu

Journal of Scientific Computing

ISSN 0885-7474
Volume 51
Number 3

J Sci Comput (2012) 51:527-559
DOI 10.1007/s10915-011-9520-4

Springer

J Sci Comput (2012) 51:527–559
DOI 10.1007/s10915-011-9520-4

Hybrid Well-balanced WENO Schemes with Different Indicators for Shallow Water Equations

Gang Li · Changna Lu · Jianxian Qiu

Received: 23 April 2011 / Revised: 4 July 2011 / Accepted: 12 July 2011 / Published online: 2 August 2011

Abstract In (J. Comput. Phys. 229: 8105–8129, 2010), Li and Qiu investigated the hybrid weighted essentially non-oscillatory (WENO) schemes with different indicators for Euler equations of gas dynamics. In this continuation paper, we extend the method to solve the one- and two-dimensional shallow water equations with source term due to the non-flat bottom topography, with a goal of obtaining the same advantages of the schemes for the Euler equations, such as the saving computational cost, essentially non-oscillatory property for general solution with discontinuities, and the sharp shock transition. Extensive simulations in one- and two-dimensions are provided to illustrate the behavior of this procedure.

Keywords WENO approximation · Up-wind linear approximation · Troubled-cell indicator · Shallow water equations · Hybrid schemes · Source term

The research was partially supported by NSFC 10931004, 40906048 and Science research fund of Nanjing University of Information Science & Technology 20090203.

G. Li · J. Qiu
Department of Mathematics, Nanjing University, Nanjing, Jiangsu 210093, P.R. China

J. Qiu
e-mail: jxqiu@nju.edu.cn

G. Li
e-mail: gangli1978@163.com

G. Li
School of Mathematical Science, Qingdao University, Qingdao, Shandong 266071, P.R. China

C. Lu
College of Mathematics & Physics, Nanjing University of Information Science & Technology, Nanjing, Jiangsu 210044, P.R. China
e-mail: luchangna@nuist.edu.cn

J. Qiu (✉)
School of Mathematical Sciences, Xiamen University, Xiamen, Fujian 361005, P.R. China
e-mail: jxqiu@xmu.edu.cn

1 Introduction

In this continuous paper, we extend the hybrid weighted essentially non-oscillatory schemes with different indicators which were investigated by Li and Qiu [11] for Euler equations of the gas dynamics, to solve the one- and two-dimensional shallow water equations with source term due to the non-flat bottom topography.

The shallow water equations, also referred to as the Saint-Venant system, have a wide applications in hydraulic and coastal engineering, e.g., tidal flows in estuary and coastal water regions, bore wave propagation, the stationary hydraulic jump and river, reservoir and open channel flow, etc. The shallow water equations govern the flow of an incompressible fluid with free surface when the depth of the fluid is small when compared to the characteristic dimension of the problem. This system describes the flow as a conservation laws with additional source term. These equations are obtained from the incompressible Euler equations assuming that the pressure is hydrostatic and neglecting dissipative effects. The one-dimensional shallow water equations take the following form:

$$\begin{cases} h_t + (hu)_x = 0, \\ (hu)_t + (hu^2 + \frac{1}{2}gh^2)_x = -ghb_x, \end{cases} \tag{1.1}$$

where h, u are the water depth and water velocity, respectively; g is the gravitational constant; $b = b(x)$ denotes the bottom topography. For the homogeneous case, the performance of the shallow water equations is similar to that of the compressible Euler equations in aerodynamics. A lot of shock and discontinuity capture methods that are well developed in aerodynamics can be used to solve the shallow water equations, including the cases with strong discontinuity. However, the presence of the source term changes the property of the system considerably. Here, for simplicity, we only consider the source term due to the bottom topography (non-flat bottom). Other effects, such as friction on the bottom topography and on the surface, wind forces, as well as variations of the channel width, can also result in the additional source term. There are considerable efforts in the literature which have been devoted to the development of the numerical methods to the conservation system with source term (also called balance laws). In 1994, Bermudez and Vazquez [2] firstly proposed the idea of the "exact conservation property" (exact C-property), which means that a scheme is exactly compatible with the quiescent flow $h + b = \text{constant}$ and $hu = 0$. This property is necessary for the balancing between the flux gradient and the source term. An efficient scheme should satisfy this property, and is termed as well-balanced scheme. Vukovic and Sopta [19] incorporated the exact C-property into the essentially nonoscillatory (ENO) and WENO schemes. Later, Crnjaric, Vukovic and Sopta [5] extended the property to the bed-load sediment transport equation and presented schemes that achieved balance between the flux gradient and the nonconservative product term. Rogers [14] presented an algebraic technique for the balancing between the flux gradient and the source term. The main idea is to mathematically rearrange the shallow water equations to be balanced when Roe's approximation Riemann solver is applied in finite volume framework. Unfortunately, most of the works mentioned above can not obtain the expected accuracy and handle the complicated bottom topography simultaneously.

In order to overcome the drawback, Xing and Shu [20] introduced the high order well-balanced finite difference WENO schemes, which can maintain the exact C-property and be genuine high order accuracy for the general solutions of the shallow water equations. The main idea of [20] is a special decomposition of the source term, such that a discretization of the source term can be both high order accurate for the general solutions and exactly well

balanced with the flux gradient for stationary flow. In 2006, Xing and Shu extended this idea of decomposition of source term to a general class of balance laws in the framework of finite difference schemes [21], and in the framework of finite volume methods and Runge-Kutta discontinuous Galerkin (RKDG) finite element methods [22]. More recently, Xing et al. [23] designed a positivity-preserving high order well-balanced discontinuous Galerkin methods for the shallow water equations. Their methods can maintain the well balancing between the flux gradient and the source term, and preserve the positivity of the water depth. It is desirable that the numerical methods can handle the dry/wet fronts efficiently.

However, the high order well-balanced finite difference WENO schemes for the shallow water equations have a drawback, which is the same as that of finite difference WENO schemes for the Euler equations of gas dynamics, i.e., the computational cost is very expensive. The drawback is mainly due to the computation of nonlinear weights and the local characteristic decomposition procedure.

In [11], Li and Qiu investigated a hybrid version of WENO schemes with high order up-wind linear schemes (we call it hybrid WENO schemes) for the Euler equations. The main idea of the schemes is to identify discontinuity by a discontinuity indicator, then reconstruct the numerical flux by WENO approximation in discontinuous regions and by up-wind linear approximation in smooth regions in which the local characteristic decompositions and the nonlinear weights for part of the procedure are avoided, hence the hybrid scheme can reduce the computational cost while still maintaining non-oscillatory properties for problems with strong discontinuity. An important component of the hybrid scheme is the indicator to automatically identify where the discontinuity of the solution is. These indicators are mainly based on the troubled-cell indicators for the discontinuous Galerkin (DG) finite element methods, are also called limiters, which are listed in [13] by Qiu and Shu. Recently, Zhu and Qiu used these limiters as troubled-cell indicators for adaptive RKDG methods in [25]. In [11], by comparing different indicators for the one-dimensional Euler equations, we choose four better indicators: troubled-cell indicator based on the average total variation of the solution (ATV), the minmod-based TVB limiter (TVB) [3], multi-resolution analysis of Harten (MR) [7] and a shock-detection technique by Krivodonova et al. (KXRCF) [9]. They result in less CPU time, smaller percentage of reconstruction of fluxes by WENO approximation and more accurate numerical solutions. Subsequently, we apply the better indicators to the two-dimensional case. Extensive numerical experiments of one- and two-dimensional Euler equations suggest that the hybrid WENO schemes with discontinuity indicators can save the computational cost considerably while maintaining the non-oscillatory property for general solution with discontinuities and the sharp shock transition.

In this paper, we apply the hybrid WENO schemes for the shallow water equations with source term due to the non-flat bottom topography in the hope of obtaining the same properties as those of the hybrid WENO schemes in [11]. Due to the page limitation, we only consider the better indicators mentioned in [11]: ATV, TVB, MR and KXRCF.

The outline of this paper is as follows. In Sect. 2, we describe the hybrid well-balanced finite difference WENO schemes with high order up-wind linear schemes. Extensive one- and two-dimensional numerical examples are presented to demonstrate the validation of this scheme, addressing the issues of efficiency (less CPU time and smaller percentage of reconstruction of numerical fluxes by WENO approximation), non-oscillatory property in Sect. 3, and concluding remarks are given in Sect. 4.

2 Description of Hybrid Well-balanced WENO Schemes with High Order Up-wind Linear Schemes

In this section, we present hybrid well-balanced finite difference WENO schemes with high order up-wind linear schemes for the shallow water equations on non-flat bottom topography.

2.1 A Review of Well-balanced WENO Schemes

In this subsection, we give a short overview of the well-balanced WENO schemes [20].

For simplicity, we take the one-dimensional case as an example. At first, as in [20], we split the source term $-ghb_x$ into two terms $(\frac{1}{2}gb^2)_x - g(h+b)b_x$. Therefore the original equations (1.1) become

$$\begin{cases} h_t + (hu)_x = 0, \\ (hu)_t + (hu^2 + \frac{1}{2}gh^2)_x = (\frac{1}{2}gb^2)_x - g(h+b)b_x, \end{cases} \tag{2.1}$$

which can be denoted by

$$U_t + f(U)_x = G_1 + G_2,$$

where $U = (h, hu)^T$, $f(U) = (hu, hu^2 + \frac{1}{2}gh^2)^T$, $G_1 = (0, (\frac{1}{2}gb^2)_x)^T$, $G_2 = (0, -g(h+b)b_x)^T$. This special splitting in the source term of (2.1) is crucial for the design of the well-balanced WENO schemes.

We consider a numerical scheme for (2.1). A scheme is called a *linear scheme* if all the spatial derivatives are approximated by a linear finite difference operator. A linear finite difference operator D is defined as that one can satisfy

$$D(\alpha f_1 + \beta f_2) = \alpha D(f_1) + \beta D(f_2) \tag{2.2}$$

for any constants α, β and grid functions f_1 and f_2.

However, the WENO schemes are nonlinear. The nonlinearity comes from the nonlinear weight, which in turn comes from the nonlinearity of the smoothness indicators. In order to construct a linear scheme which can maintain the exact C-property even with the presence of the nonlinearity of the nonlinear weight. Xing and Shu [20] adopted the following procedures, so that the exact C-property is maintained and accuracy and nonlinear stability are not affected.

To present their basic ideas, we firstly considered the situation when the WENO scheme is applied without the flux splitting and the local characteristic decomposition.

For the still water stationary solutions of (2.1), we have

$$h + b = \text{constant} \quad \text{and} \quad hu = 0. \tag{2.3}$$

For any consistent linear scheme, the first equation $(hu)_x$ will not impose any difficulties. The WENO approximation to d_x with $d = hu^2 + \frac{1}{2}gh^2$ can be eventually written as

$$d_x|_{x=x_j} \approx \sum_{k=-r-1}^{r+1} a_k d_{j+k} \equiv D_d(d)_j. \tag{2.4}$$

For the approximation to $(\frac{1}{2}gb^2)_x$ and b_x in the source term of (2.1), they use the finite difference operator D_d where $d = hu^2 + \frac{1}{2}gh^2$ is fixed, namely to use the same coefficients a_k obtained from the smoothness indicators of $d = hu^2 + \frac{1}{2}gh^2$. So

$$\left(\frac{1}{2}gb^2\right)_x|_{x=x_j} \approx \sum_{k=-r-1}^{r+1} a_k \left(\frac{1}{2}gb^2\right)_{j+k} \equiv D_d\left(\frac{1}{2}gb^2\right), \tag{2.5}$$

$$b_x|_{x=x_j} \approx \sum_{k=-r-1}^{r+1} a_k b_{j+k} \equiv D_d(b)_j. \tag{2.6}$$

By the minor modifications, we observe that the finite difference operator D_d with the coefficient a_k based on the smoothness indicators of $d = hu^2 + \frac{1}{2}gh^2$ fixed is a linear finite difference operator which satisfy (2.2). Thus the second equation has the truncation error

$$D_d\left(hu^2 + \frac{1}{2}gh^2\right) - D_d\left(\frac{1}{2}gb^2\right) + g(h+b)D_d(b) = 0.$$

Proposition 2.1 *Linear schemes for the shallow water equations* (2.1) *for the still water stationary solutions* (2.3) *can maintain the exact C-property* [20].

Moreover, the WENO schemes with flux splitting and local characteristic field decomposition maintain the exact C-property, see [20] for more details. In addition, here the flux splitting is taken a modification, i.e.,

$$f^{\pm}(U) = \frac{1}{2}\left[\begin{pmatrix} hu \\ hu^2 + \frac{1}{2}gh^2 \end{pmatrix} \pm \alpha_i \begin{pmatrix} h+b \\ hu \end{pmatrix}\right], \tag{2.7}$$

where

$$\alpha_i = \max_u |\lambda_i(u)| \tag{2.8}$$

with $\lambda_i(u)$ being the ith eigenvalue of the Jacobian matrix $f'(U)$. This minor modification is justified since b does not depend on the time t. Similar technique is used in the surface gradient method of Zhou et al. [24].

The basic idea is to use the linear finite difference operator D_d in (2.4) with nonlinear weights whose smoothness indicators obtained from $f^{\pm}(U)$ in (2.7) fixed, and apply the operator D_d to approximate $(0, \frac{1}{2}gb^2)_x^T$ and $(0, b)_x^T$ in the source term. This amounts to split the two derivatives in the source term as

$$\begin{pmatrix} 0 \\ \frac{1}{2}gb^2 \end{pmatrix}_x = \frac{1}{2}\begin{pmatrix} 0 \\ \frac{1}{2}gb^2 \end{pmatrix}_x + \frac{1}{2}\begin{pmatrix} 0 \\ \frac{1}{2}gb^2 \end{pmatrix}_x, \quad \begin{pmatrix} 0 \\ b \end{pmatrix}_x = \frac{1}{2}\begin{pmatrix} 0 \\ b \end{pmatrix}_x + \frac{1}{2}\begin{pmatrix} 0 \\ b \end{pmatrix}_x \tag{2.9}$$

and apply the same flux splitting WENO procedure to approximate them i.e., one half part of each source term is approximated by the linear finite difference operator D_d with coefficients a_k obtained from the computation of $f^+(U)$, and the remaining part by the linear finite difference operator D_d with coefficients a_k obtained from the computation of $f^-(U)$. We refer to [20] for more details.

Remark 1 Especially, the well-balanced WENO schemes reduce to the original WENO schemes [8, 16, 17], when the bottom topography is flat ($b = 0$), i.e., free of source term.

Remark 2 For the two-dimensional case

$$\begin{pmatrix} h \\ hu \\ hv \end{pmatrix}_t + \begin{pmatrix} hu \\ hu^2 + \frac{1}{2}gh^2 \\ huv \end{pmatrix}_x + \begin{pmatrix} hv \\ huv \\ hv^2 + \frac{1}{2}gh^2 \end{pmatrix}_y = \begin{pmatrix} 0 \\ -ghb_x \\ -ghb_y \end{pmatrix}, \tag{2.10}$$

where u and v are the water velocity in x- and y-direction, respectively, the source term are again split as for the one-dimensional case

$$-ghb_x = \left(\frac{1}{2}gb^2\right)_x - g(h+b)b_x, -ghb_y = \left(\frac{1}{2}gb^2\right)_y - g(h+b)b_y.$$

2.2 Description of the Discontinuity Indicators

In this subsection we give a brief review of the better discontinuity indicators which give better performances than other indicators in [11].

For convenience of presentation of the discontinuity indicators, we construct a quadratic polynomial on cell $[x_{j-1/2}, x_{j+1/2}]$ at time step t_n, denoted by $P_2(x)$:

$$P_2(x) = u_j^{(0)} + u_j^{(1)}\frac{x - x_j}{\Delta x} + u_j^{(2)}\left[\left(\frac{x - x_j}{\Delta x}\right)^2 - \frac{1}{12}\right], \quad x \in [x_{j-1/2}, x_{j+1/2}],$$

such that

$$P_2(x_k) = u_k^n, \quad k = j-1, j, j+1,$$

we have:

$$u_j^{(0)} = \frac{1}{24}(u_{j-1}^n + 22u_j^n + u_{j+1}^n), \quad u_j^{(1)} = \frac{1}{2}(u_{j+1}^n - u_{j-1}^n), \quad u_j^{(2)} = \frac{1}{2}(u_{j-1}^n - 2u_j^n + u_{j+1}^n).$$

Now we describe different discontinuity indicators in detail:

1. Discontinuity indicator based on the average total variation of the solution. (ATV, we will use the same abbreviation as in [13, 25] for each indicator). Let TV denote the total variation of the solution at time step t_n,

$$TV \equiv TV(u^n) = \sum_j |u_{j+1}^n - u_j^n|.$$

If $|u_{j+1}^n - u_j^n| \geq \theta\frac{TV}{N}$, we declare that in cell $[x_j, x_{j+1}]$ the solution has a discontinuity, and cells I_j and I_{j+1} are identified as troubled cells. Here N is the number of cells. $0 < \theta < 1$ a constant, is the ATV parameter. The choice of θ depends on the solution. It is common in the literature to look at the variation of the solution in order to indicate the presence of discontinuities at a particular location [4, 12]. Moreover this simple definition of the discontinuity guarantees that both shock waves and contact discontinuities are properly identified. But it is difficult to choose θ accurately, for θ is problem-dependent. If θ is chosen too small, this will increase computational cost unnecessarily; however if θ is chosen too large, spurious oscillations will appear.
2. The minmod-based TVB limiter [3] (TVB). Let

$$\tilde{u}_j = P_2(x_{j+1/2}) - u_j^{(0)}, \quad \tilde{\tilde{u}}_j = -P_2(x_{j-1/2}) + u_j^{(0)}.$$

These are modified by the modified minmod function

$$\begin{aligned} \tilde{u}_j^{(mod)} &= \tilde{m}(\tilde{u}_j, u_{j+1}^{(0)} - u_j^{(0)}, u_j^{(0)} - u_{j-1}^{(0)}), \\ \tilde{\tilde{u}}_j^{(mod)} &= \tilde{m}(\tilde{\tilde{u}}_j, u_{j+1}^{(0)} - u_j^{(0)}, u_j^{(0)} - u_{j-1}^{(0)}), \end{aligned} \tag{2.11}$$

where $\tilde{m}$ is given by

$$\tilde{m}(a_1, a_2, \ldots, a_n) = \begin{cases} a_1 & \text{if } |a_1| \le M(\Delta x)^2, \\ m(a_1, a_2, \ldots, a_n) & \text{otherwise,} \end{cases} \tag{2.12}$$

and the minmod function m is given by

$$m(a_1, a_2, \ldots, a_n) = \begin{cases} s \cdot \min_{1 \le j \le n} |a_j| & \text{if } sign(a_1) = sign(a_2) = \cdots = sign(a_n) = s, \\ 0 & \text{otherwise.} \end{cases} \tag{2.13}$$

The TVB limiter parameter $M > 0$ is a constant.

If $\tilde{u}_j^{(mod)} \ne \tilde{u}_j$ or $\tilde{\tilde{u}}_j^{(mod)} \ne \tilde{\tilde{u}}_j$, we declare the cell I_j as a discontinuous cell.

Unfortunately, the TVB limiter parameter M is dependent on the problem. There is no automatic switch which works well for various situations. For scalar problems it is possible to estimate M by the initial condition as in [3] (M is proportional to the second derivative of the initial data at smooth extrema), however it is difficulty to estimate M for system of equations. If M is chosen too small, more cells containing discontinuities will be identified than necessary, therefore increasing computational cost; however if M is chosen too large, spurious oscillations will appear.

3. Multi-resolution analysis of Harten [7] (MR). Given the point values $\{u_j\}_0^N$ of function $u(x)$. Let $\tilde{u}_j$ denote the approximation to u_j which is obtained from the unique polynomial $\tilde{u}(x)$ of degree one that interpolates $u(x)$ at $x_{j-1},\ x_{j+1}$,

$$\tilde{u}_j = \tilde{u}(x_j) = \frac{1}{2}(u_{j-1} + u_{j+1}),$$

and let d_j denote the corresponding approximation error:

$$d_j = u_j - \tilde{u}_j.$$

If $u(x)$ at $x = \bar{x}$ has $p-1$ continuous derivatives and a jump discontinuity in its p-th derivative as denoted by $[\cdot]$, then for x_j near $\bar{x}$

$$d_j \approx \begin{cases} (\Delta x)^p [u^{(p)}], & p \le 2, \\ (\Delta x)^2 u^{(2)}, & p \ge 2. \end{cases} \tag{2.14}$$

In this paper, if $|d_j| \ge \varepsilon_{MR} \Delta x$, the cell I_j is identified as a discontinuous cell, here ε_{MR} is a multi-resolution parameter.

4. A shock-detection technique by Krivodonova et al. [9] (KXRCF). Partition the boundary of a cell I_j into two portions ∂I_j^- and ∂I_j^+, where the flow is into ($\vec{v} \cdot \vec{n} < 0$, $\vec{n}$ is the normal vector to ∂I_j) and out of ($\vec{v} \cdot \vec{n} > 0$) I_j, respectively. The cell I_j is identified as a discontinuous cell, if

$$\frac{|\int_{\partial I_j^-} (u^h|_{I_j} - u^h|_{I_{n_j}}) ds|}{h_j^{\frac{k+1}{2}} |\partial I_j^-| \|u^h|_{I_j}\|} > 1, \tag{2.15}$$

here h_j is the radius of the circumscribed circle in the element I_j. I_{n_j} is the neighbor of I_j on the side of ∂I_j^- and the norm is based on an element average in one-dimensional case.

Remark 3 We summarize the relevant properties of the solution to the two-dimensional shallow water equations? For detail, we refer to [18].

- The left and right waves for x-direction or the bottom and top waves for y-direction, are either shock or rarefaction waves and the middle wave is always a shear wave.
- For x-direction, across the left and right waves both h and u change but v remains constant; across the middle wave v changes discontinuously both h and u remain constant. The property is similar for y-direction.

Consequently, for the one-dimensional shallow water equations, we use the water depth h and the water velocity u at the same time as indicator variables to identify the discontinuities.

For the two-dimensional case, the discontinuity indicators work in x- and y-direction, respectively, to identify the discontinuities. For the x-direction, we use the water depth h and the water x-velocity u to identify the discontinuity, and for the y-direction, we apply the water depth h and the water y-velocity to detect the discontinuities.

2.3 Algorithm of Hybrid Well-balanced WENO Schemes

The procedure of the $(2r+1)$th-order well-balanced WENO schemes with the $(2r+1)$th-order up-wind linear schemes is then presented in the following.

Step 1. The discontinuity indicator is applied to identify troubled cell, namely the locations of discontinuity of the numerical solution, only once at the beginning of the Runge-Kutta time discretization procedure.

Step 2. Reconstruction of the numerical flux based on either the $(2r+1)$th-order WENO approximation in the discontinuous vicinage or the $(2r+1)$th-order up-wind linear approximation in the smooth vicinage. The numerical fluxes $\hat{f}^+_{j+1/2}$ and $\hat{f}^-_{j-1/2}$ will be reconstructed by WENO approximations in the stencils which contain a troubled cell identified in the Step 1. For example, let I_{j_0} to be a troubled cell, then there are $(2r+1)$ stencils $\{x_{j_0-r+l},\ldots,x_{j_0+r+l}\}, l=-r,\ldots,r$ which contain a discontinuity, the numerical fluxes $\hat{f}^+_{j_0+l+1/2}$ and $\hat{f}^-_{j_0+l-1/2}, l=-r,\ldots,r$ will be reconstructed by the $(2r+1)$ order WENO approximation in these stencils. And the numerical fluxes $\hat{f}^+_{j_0+l+1/2}$ and $\hat{f}^-_{j_0+l-1/2}, l=-r,\ldots,r$ will be reconstructed by the $(2r+1)$ order up-wind linear approximation in the stencils which do not contain any troubled cells. Finally, we obtain the numerical fluxes $\hat{f}_{j+1/2}=\hat{f}^+_{j+1/2}+\hat{f}^-_{j+1/2}$, in which $\hat{f}^+_{j+1/2}$, $\hat{f}^-_{j+1/2}$ are reconstructed by WENO approximation or up-wind linear approximation.

Step 3. The approximation to the derivatives in the source term is constructed with splitting (2.9) as the above procedure accordingly.

2.4 The Procedure for the Reconstruction of Numerical Flux

In this subsection we describe the reconstruction for the numerical flux by the WENO approximation and the high order up-wind linear approximation.

We start with the description for the one-dimensional case. Given grid points $\{x_j\}$, we define cell size, cell center and cell by $\Delta x = x_{j+1}-x_j$, $x_{j+1/2}=x_j+\Delta x/2$ and $I_j =$

$[x_{j-1/2}, x_{j+1/2}]$, respectively. For the shallow water equations on non-flat bottom topography (2.1), we must obtain the numerical flux $\hat{f}_{j+1/2}$ to approximate $f(U)_x$, so that

$$f(U)_x|_{x=x_j} \approx \frac{\hat{f}_{j+1/2} - \hat{f}_{j-1/2}}{\Delta x}.$$

We take the reconstruction for the numerical flux of one-dimensional scalar conservation laws as an example. The numerical flux $\hat{f}_{j+1/2}$ approximates $h_{j+1/2} = h(x_{j+1/2})$ to a high order accuracy with $h(x)$ implicitly defined as in [8, 16]

$$f(u(x)) = \frac{1}{\Delta x} \int_{x-\Delta x/2}^{x+\Delta x/2} h(\xi) d\xi. \tag{2.16}$$

To take up-winding into account, we split a general flux into two parts either globally or locally

$$f(u) = f^+(u) + f^-(u), \tag{2.17}$$

where $df^+(u)/du \geq 0$ and $df^-(u)/du \leq 0$. For simplicity, we define

$$f^{\pm}(u) = \frac{1}{2}(f(u) \pm \alpha u), \tag{2.18}$$

where $\alpha = \max_u |f'(u)|$ are the maximum is taken over the whole relevant range of u. This is the global Lax-Friedrichs flux splitting. The numerical fluxes $\hat{f}^+_{j+1/2}$ and $\hat{f}^-_{j+1/2}$ are relative to $f^+(u)$ and $f^-(u)$, respectively and will be reconstructed by either WENO approximation in the discontinuous regions or high order up-wind linear approximation in the smooth regions. Then we have the numerical flux

$$\hat{f}_{j+1/2} = \hat{f}^+_{j+1/2} + \hat{f}^-_{j+1/2}.$$

We only present the procedure for the reconstruction of the numerical flux $\hat{f}^+_{j+1/2}$. The formulae for the negative part of the split flux are symmetric (with respect to $x_{j+1/2}$) and will not be presented.

The key idea of the WENO approximation is a convex combination of lower order fluxes based on candidate stencils $S_k = \{x_{j+k-r}, \ldots, x_{j+k}\}, k = 0, 1, \ldots, r$ to obtain a higher order approximation. The choice of the weight ω_k to each candidate stencil, which is a *nonlinear* function of the grid values, is crucial to the success of the WENO approximation. For more discussions of the WENO approximation to $\hat{f}^+_{j+1/2}$, we refer to [8, 16, 17].

For the high order up-wind linear approximation, we use all the r candidate stencils $S_k = \{x_{j+k-r}, \ldots, x_{j+k}\}, k = 0, 1, \ldots, r$, i.e., $S = \bigcup_{k=0}^{r} S_k$, which contains $(2r+1)$ grid point values of $f^+(u)$, to obtain a $(2r+1)$th-order approximation to $\hat{f}^+_{j+1/2}$ in smooth regions such that

$$\frac{1}{\Delta x} \int_{I_i} q_r^{2r+1}(x) dx = f_i^+, \quad i = j-r, \ldots, j+r,$$

and

$$\hat{f}^+_{j+1/2} = q_r^{2r+1}(f^+_{j-r}, \ldots, f^+_{j+r}) = \sum_{l=0}^{2r} b_l f^+_{j+l-r}, \tag{2.19}$$

where $b_l, 0 \le l \le 2r$ are constant coefficients, for details, we refer to [16]. By simple algebra operation, we get

$$\hat{f}^+_{j+1/2} = q_r^{2r+1}(f^+_{j-r}, \ldots, f^+_{j+r}) = \sum_{k=0}^{r} C_k^r q_k^r (f^+_{j+k-r}, \ldots, f^+_{j+k}), \tag{2.20}$$

where the coefficient C_k^r is the *linear weight* and in smooth regions $\omega_k = C_k^r + \mathcal{O}(\Delta x^r), k = 0, 1, \ldots, r$. Thus C_k^r bear the name of *optimal weight*.

With the numerical flux $\hat{f}_{j+1/2} = \hat{f}^+_{j+1/2} + \hat{f}^-_{j+1/2}$ based on the WENO approximation and the high order up-wind linear approximation, we can approximate

$$f(u)_x|_{x=x_j} \approx \frac{\hat{f}_{j+1/2} - \hat{f}_{j-1/2}}{\Delta x}.$$

For the one-dimensional system of shallow water equations on non-flat bottom topography (2.1), we can similarly approximate $f(U)_x|_{x=x_j}$ with the modified flux splitting (2.7). In addition, in order to achieve better qualities at the price of more complicated computations, the WENO approximation is always used with a local characteristic decomposition, see [16] for details, while the up-wind linear approximation is used component by component. Similarly, we can approximate the two derivatives in the source term $(0, \frac{1}{2}gb^2)^T_x$ and $(0, b)^T_x$ with splitting (2.9) as the procedure for the approximation to $f(U)_x$.

Now, we consider that whether the hybrid well-balanced WENO scheme can maintain the exact C-property.

Firstly, in the discontinuous regions, the hybrid well-balanced WENO scheme is in fact the well-balanced WENO scheme of Xing and Shu [20], so it can maintain the exact C-property, we refer to [20] for further discussions.

Subsequently, we consider the hybrid well-balanced WENO scheme in the smooth regions. Here the scheme is the component-wise up-wind linear scheme without local characteristic decomposition. Now the flux $f(U)$ is written as a sum of $f^+(U)$ and $f^-(U)$, where $f^+(U)$ and $f^-(U)$ are the modified flux splitting in (2.7). For the still water stationary solution (2.3), by the consistency of the up-wind linear scheme, the effect of the viscosity term $\pm\alpha_i \binom{h+b}{hu}$ towards the approximation to $f(U)_x$ is zero. So, it is clear that (2.4) with $d = (hu, hu^2 + \frac{1}{2}gh^2)^T$ being a vector grid function can represent a flux splitting up-wind linear approximation, with a simple splitting $f^\pm(U) = \frac{1}{2}f(U)$, and a_k being 2×2 matrices depending linearly on the constant coefficients of the $(2r+1)$th-order fixed stencil approximation to $f^\pm(U)$. The key idea now is to use the difference operator D_d of (2.4) and apply it to approximate $(0, \frac{1}{2}gb^2)^T_x$ and $(0, b)^T_x$ with the splitting in (2.9). We can prove the component-wise up-wind linear scheme with flux splitting and with the special handling of the source term described in (2.9) is a linear scheme, so it can maintain the exact C-property.

At last, we consider the hybrid well-balanced WENO scheme at the interface between the smooth and the discontinuous regions. Without loss of generality, we assume that the positive part and the negative part of the numerical flux $\hat{f}_{j+1/2}$ are from the component-wise up-wind linear approximation and the WENO approximation with local characteristic decomposition, respectively. We denote both the parts by $\hat{f}^{+,uw}_{j+1/2}$ and $\hat{f}^{-,\mathrm{WENO}}_{j+1/2}$, respectively. At the same time we assume that the positive and the negative parts of the numerical flux $\hat{f}_{j-1/2}$ are all from the component-wise up-wind linear approximation and denoted by $\hat{f}^{+,uw}_{j-1/2}$ and $\hat{f}^{-,uw}_{j-1/2}$, respectively.

$\hat{f}^{+,uw}_{j+1/2}$ can be written out in the following form

$$\begin{aligned}\hat{f}^{+,uw}_{j+1/2} &= \sum_{k=-r}^{r} c_k f^+_{j+k} \\ &= \sum_{k=-r}^{r} c_k \frac{1}{2}(f_{j+k} + \alpha U_{j+k}) \\ &= \frac{1}{2}\sum_{k=-r}^{r} c_k f_{j+k} + \frac{1}{2}\sum_{k=-r}^{r} c_k(\alpha U_{j+k}),\end{aligned} \tag{2.21}$$

where $f^+ = f^+(U)$ is defined in (2.7) with $U = (h+b, hu)^T$ and $f = f(U) = (hu, hu^2 + \frac{1}{2}gh^2)^T$ being vector grid functions, c_k are 2×2 diagonal matrices depending linearly on the constant coefficients of the $(2r+1)$th-order fixed stencil approximation to f^+ on the stencil $\{x_{j-r}, \ldots, x_{j+r}\}$, and α is a 2×2 diagonal matrix involving α_i in (2.8).

$\hat{f}^{-,\mathrm{WENO}}_{j+1/2}$ can be written out as follows

$$\begin{aligned}\hat{f}^{-,\mathrm{WENO}}_{j+1/2} &= \sum_{k=-r+1}^{r+1} a_k f^-_{j+k} \\ &= \sum_{k=-r+1}^{r+1} a_k \frac{1}{2}(f_{j+k} - \alpha U_{j+k}) \\ &= \frac{1}{2}\sum_{k=-r+1}^{r+1} a_k f_{j+k} - \frac{1}{2}\sum_{k=-r+1}^{r+1} a_k(\alpha U_{j+k}),\end{aligned} \tag{2.22}$$

where $f^- = f^-(U)$ is defined in (2.7) with $U = (h+b, hu)^T$ and $f = f(U) = (hu, hu^2 + \frac{1}{2}gh^2)^T$ being vector grid functions, a_k are 2×2 matrices depending nonlinearly on the smoothness indicators of f^-, and α is also a 2×2 diagonal matrix involving α_i in (2.8).

So we have

$$\hat{f}^{hybrid}_{j+1/2} = \hat{f}^{+,uw}_{j+1/2} + \hat{f}^{-,\mathrm{WENO}}_{j+1/2}. \tag{2.23}$$

Similarly, $\hat{f}^{+,uw}_{j-1/2}$ has the following form

$$\begin{aligned}\hat{f}^{+,uw}_{j-1/2} &= \sum_{k=-r-1}^{r-1} \hat{c}_k f^+_{j+k} \\ &= \sum_{k=-r-1}^{r-1} \hat{c}_k \frac{1}{2}(f_{j+k} + \alpha U_{j+k}) \\ &= \frac{1}{2}\sum_{k=-r-1}^{r-1} \hat{c}_k f_{j+k} + \frac{1}{2}\sum_{k=-r-1}^{r-1} \hat{c}_k(\alpha U_{j+k}),\end{aligned} \tag{2.24}$$

where $f^+ = f^+(U)$ is defined in (2.7) with $U = (h+b, hu)^T$ and $f = f(U) = (hu, hu^2 + \frac{1}{2}gh^2)^T$ being vector grid functions, $\hat{c}_k$ are 2×2 diagonal matrices depending linearly on the constant coefficients of the $(2r+1)$th-order fixed stencil approximation to f^+ on the stencil $\{x_{j-r-1}, \ldots, x_{j+r-1}\}$, and α is a 2×2 diagonal matrix involving α_i in (2.8).

$\hat{f}^{-,uw}_{j-1/2}$ can be written out in the below form

$$\begin{aligned}\hat{f}^{-,uw}_{j-1/2} &= \sum_{k=-r}^{r} c_k f^-_{j-k} \\ &= \sum_{k=-r}^{r} c_k \frac{1}{2}(f_{j-k} - \alpha U_{j-k}) \\ &= \frac{1}{2}\sum_{k=-r}^{r} c_k f_{j-k} - \frac{1}{2}\sum_{k=-r}^{r} c_k(\alpha U_{j-k}),\end{aligned} \tag{2.25}$$

where $f^- = f^-(U)$ is defined in (2.7) with $U = (h+b, hu)^T$ and $f = f(U) = (hu, hu^2 + \frac{1}{2}gh^2)^T$ being vector grid functions, c_k are the same 2×2 matrices as in (2.21), and α is a 2×2 diagonal matrix involving α_i in (2.8).

Consequently, we can obtain

$$\hat{f}^{uw}_{j-1/2} = \hat{f}^{+,uw}_{j-1/2} + \hat{f}^{-,uw}_{j-1/2}. \tag{2.26}$$

With the formulae in (2.21), (2.22), (2.24) and (2.25), the approximation to $f(U)_x$ can be written out as follows

$$\begin{aligned} f(U)_x|_{x=x_j} &\approx \frac{1}{\Delta x}(\hat{f}^{hybrid}_{j+1/2} - \hat{f}^{uw}_{j-1/2}) \\ &= \frac{1}{\Delta x}\Bigg[\Bigg(\frac{1}{2}\sum_{k=-r}^{r} c_k f_{j+k} + \frac{1}{2}\sum_{k=-r}^{r} c_k(\alpha U_{j+k}) + \frac{1}{2}\sum_{k=-r+1}^{r+1} a_k f_{j+k} \\ &\quad - \frac{1}{2}\sum_{k=-r+1}^{r+1} a_k(\alpha U_{j+k})\Bigg) \\ &\quad - \Bigg(\frac{1}{2}\sum_{k=-r-1}^{r-1} \hat{c}_k f_{j+k} + \frac{1}{2}\sum_{k=-r-1}^{r-1} \hat{c}_k(\alpha U_{j+k}) + \frac{1}{2}\sum_{k=-r}^{r} c_k f_{j-k} \\ &\quad - \frac{1}{2}\sum_{k=-r}^{r} c_k(\alpha U_{j-k})\Bigg)\Bigg] \\ &= \frac{1}{2\Delta x}\Bigg(\sum_{k=-r}^{r} c_k f_{j+k} - \sum_{k=-r-1}^{r-1} \hat{c}_k f_{j+k}\Bigg) + \frac{1}{2\Delta x}\Bigg(\sum_{k=-r+1}^{r+1} a_k f_{j+k} - \sum_{k=-r}^{r} c_k f_{j-k}\Bigg) \\ &\quad + \frac{1}{2\Delta x}\Bigg(\sum_{k=-r}^{r} c_k(\alpha U_{j+k}) - \sum_{k=-r-1}^{r-1} \hat{c}_k(\alpha U_{j+k})\Bigg) \\ &\quad + \frac{1}{2\Delta x}\Bigg(\sum_{k=-r}^{r} c_k(\alpha U_{j-k}) - \sum_{k=-r+1}^{r+1} a_k(\alpha U_{j+k})\Bigg). \end{aligned} \tag{2.27}$$

It should be noted that with $\pm\alpha U = \pm\alpha\binom{h+b}{hu}$ instead of the original $\pm\alpha\binom{h}{hu}$ in the flux splitting (2.7), the former becomes a constant vector for the still water stationary solutions (2.3). By U we denote U_{j+k} with an abuse of notation. So $\alpha U_{j+k} = \alpha U$ is also a

constant vector. Consequently

$$\begin{aligned}
&\frac{1}{2\Delta x}\left(\sum_{k=-r}^{r} c_k(\alpha U_{j+k}) - \sum_{k=-r-1}^{r-1} \hat{c}_k(\alpha U_{j+k})\right)\\
&= \frac{1}{2\Delta x}\left(\sum_{k=-r}^{r} c_k(\alpha U) - \sum_{k=-r-1}^{r-1} \hat{c}_k(\alpha U)\right)\\
&= \frac{1}{2\Delta x}\left[\left(\sum_{k=-r}^{r} c_k\right)(\alpha U) - \left(\sum_{k=-r-1}^{r-1} \hat{c}_k\right)(\alpha U)\right]\\
&= \frac{1}{2\Delta x}\big[I\cdot(\alpha U) - I\cdot(\alpha U)\big]\\
&= 0, \qquad (2.28)
\end{aligned}$$

where I is a 2×2 identity matrix, the equivalents $\sum_{k=-r}^{r} c_k = I$ and $\sum_{k=-r-1}^{r-1} \hat{c}_k = I$ are due to the consistency of the up-wind linear approximation for the still water stationary solutions (2.3). By the consistency of the up-wind linear approximation and the WENO approximation for the still water stationary solutions (2.3), and with the similar procedure as above, we can obtain

$$\frac{1}{2\Delta x}\left(\sum_{k=-r}^{r} c_k(\alpha U_{j-k}) - \sum_{k=-r+1}^{r+1} a_k(\alpha U_{j+k})\right) = 0. \qquad (2.29)$$

Consequently, the hybrid approximation to $f(U)_x$ in (2.27) can be eventually written out as

$$\begin{aligned}
f(U)_x|_{x=x_j} &\approx \frac{1}{\Delta x}(\hat{f}^{hybrid}_{j+1/2} - \hat{f}^{uw}_{j-1/2})\\
&= \frac{1}{2\Delta x}\left(\sum_{k=-r}^{r} c_k f_{j+k} - \sum_{k=-r-1}^{r-1} \hat{c}_k f_{j+k}\right)\\
&\quad + \frac{1}{2\Delta x}\left(\sum_{k=-r+1}^{r+1} a_k f_{j+k} - \sum_{k=-r}^{r} c_k f_{j-k}\right)\\
&= \sum_{k=-r-1}^{r+1} \beta_k f_{j+k}\\
&\equiv D_f(f)_j, \qquad (2.30)
\end{aligned}$$

where β_k are 2×2 matrices depending on the smoothness indicators involving f^+ and on the constant coefficients of the $(2r+1)$th-order fixed stencil approximation to $f^{\pm}$. The key idea now is to use the finite difference operator D_f and apply this finite difference operator D_f to approximate $(0, \frac{1}{2}gb^2)^T_x$ and $(0, b)^T_x$ in the source term with the special handling (2.9). A key observation is that the finite difference operator D_f with the coefficient matrices β_k fixed is a linear finite difference operator on any grid function, i.e.,

$$D_f(a_1 f_1 + a_2 f_2) = a_1 D_f(f_1) + a_2 D_f(f_2)$$

for constants a_1, a_2 and any grid functions f_1, f_2. Thus the proof of Proposition 2.1 will go through and we can prove that the hybrid well-balanced WENO schemes with the modified flux splitting (2.7) and with the special handling of the source term described in (2.9), maintain the exact C-property.

For the other cases of the hybrid well-balanced WENO schemes, we can prove the exact C-property with the similar procedure described above.

In summary, the hybrid well-balanced WENO schemes can maintain the exact C-property for the still water stationary solution (2.3).

Remark 4 For two-dimensional cases, the reconstruction of fluxes is based on dimension by dimension fashion.

3 Numerical Results

In this section we carry out extensive numerical experiments on one- and two-dimensional shallow water equations to demonstrate the performances of the hybrid well-balanced WENO schemes with the discontinuity indicators. Comparisons are concentrated mainly on the CPU time and on the percentage of reconstruction of fluxes by WENO approximation. We have checked the numerical accuracy for the hybrid schemes, we can see numerical accuracy of the four hybrid schemes is similar to that of WENO scheme as we expect, but for save space, we do not show the accuracy test results in the paper. Because the numerical results are not sensitive to the indicator parameters, so we apply the uniform parameters, i.e., $\theta = 0.9$, $M = 0.01$ and $\varepsilon_{MR} = 0.1$, respectively, in all the computations. In all the numerical examples, time discretization is by the classical forth order Runge-Kutta method [15], and the CFL number is taken as 0.6. The gravitational constant g is taken as 9.812. In all the figures, "◯" represents where the flux is reconstructed by WENO approximation.

3.1 Test for the Exact C-property

We test the exact C-property of the hybrid well-balanced WENO schemes. We choose two different bottom topographies on domain [0, 10]. The first bottom topography is smooth

$$b(x) = 5e^{-\frac{2}{5}(x-5)^2}, \tag{3.1}$$

and the second bottom topography is discontinuous

$$b(x) = \begin{cases} 4 & \text{if } 4 \le x \le 8, \\ 0 & \text{otherwise.} \end{cases} \tag{3.2}$$

The initial data are the still water stationary solutions

$$h + b = 10 \quad \text{and} \quad hu = 0.$$

This still water stationary solutions should be exactly preserved. We solve the solution up to $t = 0.5$. CPU time comparison among the original well-balanced WENO schemes and the hybrid well-balanced WENO schemes for the two different bottom topographies are given in Tables 1 and 2, respectively. From the tables, we can clearly observe that the hybrid well-balanced WENO schemes can save computational cost by 60–70% compared with

Table 1 Test for the exact C-property on smooth bottom topography (3.1), $t = 0.5$. The total CPU time of 6 runs with $n = 50 * i$ $(i = 1, \ldots, 6)$ cells, and the ratios of the total CPU time by the 3rd-, 5th-, 7th- and 9th-order hybrid well-balanced WENO schemes over that of the same order original well-balanced WENO schemes

Scheme or indicators	3rd-order		5th-order		7th-order		9th-order	
	CPU	Ratio	CPU	Ratio	CPU	Ratio	CPU	Ratio
WENO	5.19	1.00	5.30	1.00	9.20	1.00	17.22	1.00
ATV	1.98	0.38	1.98	0.37	3.23	0.35	5.61	0.33
TVB	1.08	0.21	1.08	0.20	1.36	0.15	1.77	0.10
MR	1.59	0.31	1.63	0.31	2.59	0.28	4.25	0.25
KXRCF	0.89	0.17	0.94	0.18	1.03	0.11	1.03	0.06

Table 2 Test for the exact C-property on smooth bottom topography (3.2), $t = 0.5$. The total CPU time of 6 runs with $n = 50 * i$ $(i = 1, \ldots, 6)$ cells, and the ratios of the total CPU time by the 3rd-, 5th-, 7th- and 9th-order hybrid well-balanced WENO schemes over that of the same order original well-balanced WENO schemes

Scheme or indicators	3rd-order		5th-order		7th-order		9th-order	
	CPU	Ratio	CPU	Ratio	CPU	Ratio	CPU	Ratio
WENO	5.20	1.00	5.20	1.00	9.02	1.00	17.20	1.00
ATV	1.06	0.20	1.09	0.21	1.55	0.17	2.30	0.13
TVB	1.13	0.22	1.17	0.23	1.64	0.18	2.48	0.14
MR	1.02	0.20	1.05	0.20	1.63	0.28	2.44	0.14
KXRCF	1.27	0.24	1.30	0.25	1.83	0.20	2.70	0.16

the same order original well-balanced WENO schemes. In order to show that the exact C-property is maintained even with round off error, we use single, double and quadruple precision to carry out the computation, and present the L^1 error for the water depth and the water discharge and the percentage of reconstruction of fluxes by WENO approximation by the 3rd-, 5th-, 7th- and 9th-order hybrid well-balanced WENO schemes using $n = 50 * i$ $(i = 1, \ldots, 6)$ cells for the two different bottom topographies in Figs. 1 and 2, respectively. We can clearly see that the L^1 error of the hybrid well-balanced WENO schemes is at the level of round off error for different precisions, verifying the expected exact C-property. In order to save space, in this paper we do not show the L^∞ errors which are similar to L^1 errors.

3.2 1-Rarefaction and 2-Shock Problem

We first consider a test case of one-dimensional shallow water equations (2.1) on a step bottom [1]. The computational domain is $[-10, 10]$. The bottom topography has a step

$$b(x) = \begin{cases} 0 & \text{if } x \le 0, \\ 1 & \text{otherwise,} \end{cases}$$

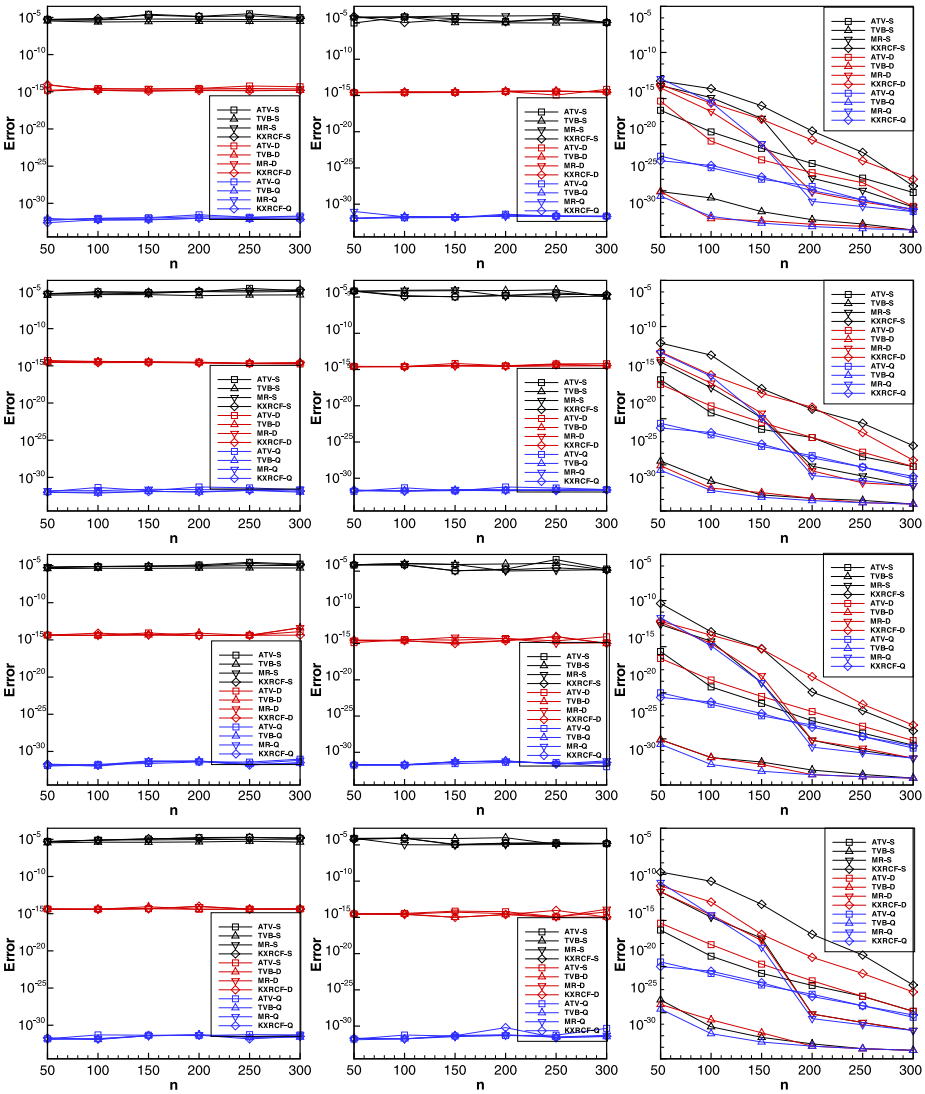

Fig. 1 Test for the exact C-property on smooth bottom topography (3.1), $t = 0.5$. L^1 error of water depth (*left*), L^1 error of water discharge (*middle*), percentage of reconstruction of fluxes by WENO approximation (*right*). From *top* to *bottom*: 3rd-, 5th-, 7th- and 9th-order schemes. "S", "D" and "Q" represent Single, Double and Quadruple precision, respectively

the initial data are as follows

$$h(x,0) = \begin{cases} 4 & \text{if } x \le 0, \\ 1 & \text{otherwise,} \end{cases} \qquad \text{and} \quad u(x,0) = 0.$$

This test case produces a 1-rarefaction spreading to the left and a 2-shock traveling right. In Table 3, we document the CPU time and the percentages of reconstruction of fluxes by WENO approximation. From Table 3, we can observe that the hybrid schemes can save com-

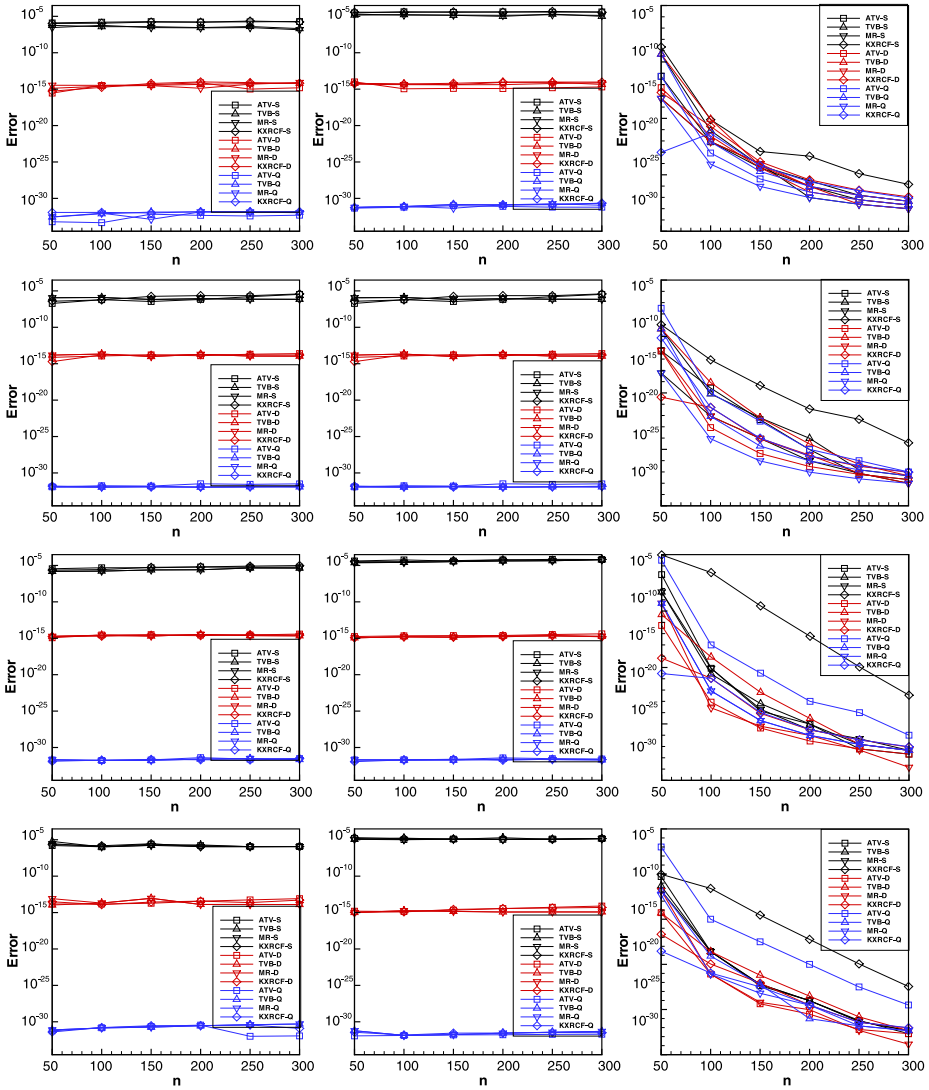

Fig. 2 Test for the exact C-property on discontinuous bottom topography (3.2), $t = 0.5$. L^1 error of water depth (*left*), L^1 error of water discharge (*middle*), percentage of reconstruction of fluxes by WENO approximation (*right*). From *top* to *bottom*: 3rd-, 5th-, 7th and 9th-order schemes. "S", "D" and "Q" represent Single, Double and Quadruple precision, respectively

putational cost by 50–60% and only about 30% reconstruction of fluxes are approximated by WENO approximation. We can also observe that the percentages of reconstruction of fluxes by WENO approximation decrease with mesh refinement in most cases, which is a very desirable property for the troubled-cell indicators. For all the indicators, we show the water surface level $h + b$, the water discharge hu at $t = 1$ against the exact solution and time history of reconstruction of fluxes by WENO approximation in Fig. 3. We can clearly observe that the numerical results for all cases keep sharp discontinuity transition

Table 3 1-rarefaction and 2-shock problem. Comparison on CPU time and percentage of reconstruction of fluxes by WENO approximation among original well-balanced WENO and hybrid well-balanced WENO schemes

N	Scheme or indicators	3rd-order		5th-order		7th-order		9th-order	
		CPU	Percent	CPU	Percent	CPU	Percent	CPU	Percent
50	WENO	0.06	100.00	0.06	100.00	0.11	100.00	0.16	100.00
	ATV	0.05	48.77	0.05	47.18	0.06	46.22	0.09	55.50
	TVB	0.05	49.14	0.06	54.17	0.08	52.72	0.09	59.77
	MR	0.03	45.34	0.05	49.39	0.09	73.95	0.14	62.83
	KXRCF	0.05	55.21	0.05	62.75	0.08	49.19	0.09	56.80
100	WENO	0.20	100.00	0.23	100.00	0.39	100.00	0.56	100.00
	ATV	0.11	33.18	0.11	31.42	0.17	31.22	0.28	40.06
	TVB	0.09	34.67	0.13	39.27	0.19	40.33	0.29	45.19
	MR	0.08	34.59	0.13	37.14	0.25	53.77	0.41	64.78
	KXRCF	0.13	41.71	0.14	40.05	0.20	40.47	0.28	44.05
200	WENO	0.80	100.00	0.89	100.00	1.50	100.00	2.25	100.00
	ATV	0.25	22.49	0.27	20.61	0.44	21.18	0.86	33.47
	TVB	0.27	21.57	0.33	25.86	0.63	32.49	0.92	35.55
	MR	0.25	24.45	0.31	25.09	0.59	30.04	0.95	37.16
	KXRCF	0.28	24.08	0.34	27.57	0.61	31.91	0.95	36.12

and are mostly oscillation-free. In order to save space, in this paper we do not show the results by the 3rd-, 7th- and 9th-order schemes which are similar to those by the 5th-order scheme.

3.3 1-Shock and 2-Shock Problem

The second test case is also on a step bottom [1]. The computational domain is $[-10, 10]$. The bottom topography is as follows

$$b(x) = \begin{cases} 0 & \text{if } x \le 0, \\ 1 & \text{otherwise}, \end{cases}$$

the initial data are given by

$$h(x,0) = \begin{cases} 4 & \text{if } x \le 0, \\ 1 & \text{otherwise}, \end{cases} \quad \text{and} \quad u(x,0) = \begin{cases} 5 & \text{if } x \le 0, \\ -0.9 & \text{otherwise}. \end{cases}$$

This test case produces two shocks: the first one moving to the left and the second one to the right. In Table 4, we document the CPU time and the percentages of reconstruction of fluxes by WENO approximation between the 3rd-, 7th-, 5th- and 9th-order original well-balanced WENO schemes and the hybrid well-balanced WENO schemes. From the Table 4, we can observe that the hybrid schemes can save the computational cost by 55–75% and only about 35% reconstruction of fluxes are approximated by WENO approximation. It is clear that the percentages of reconstruction of fluxes by WENO approximation decrease

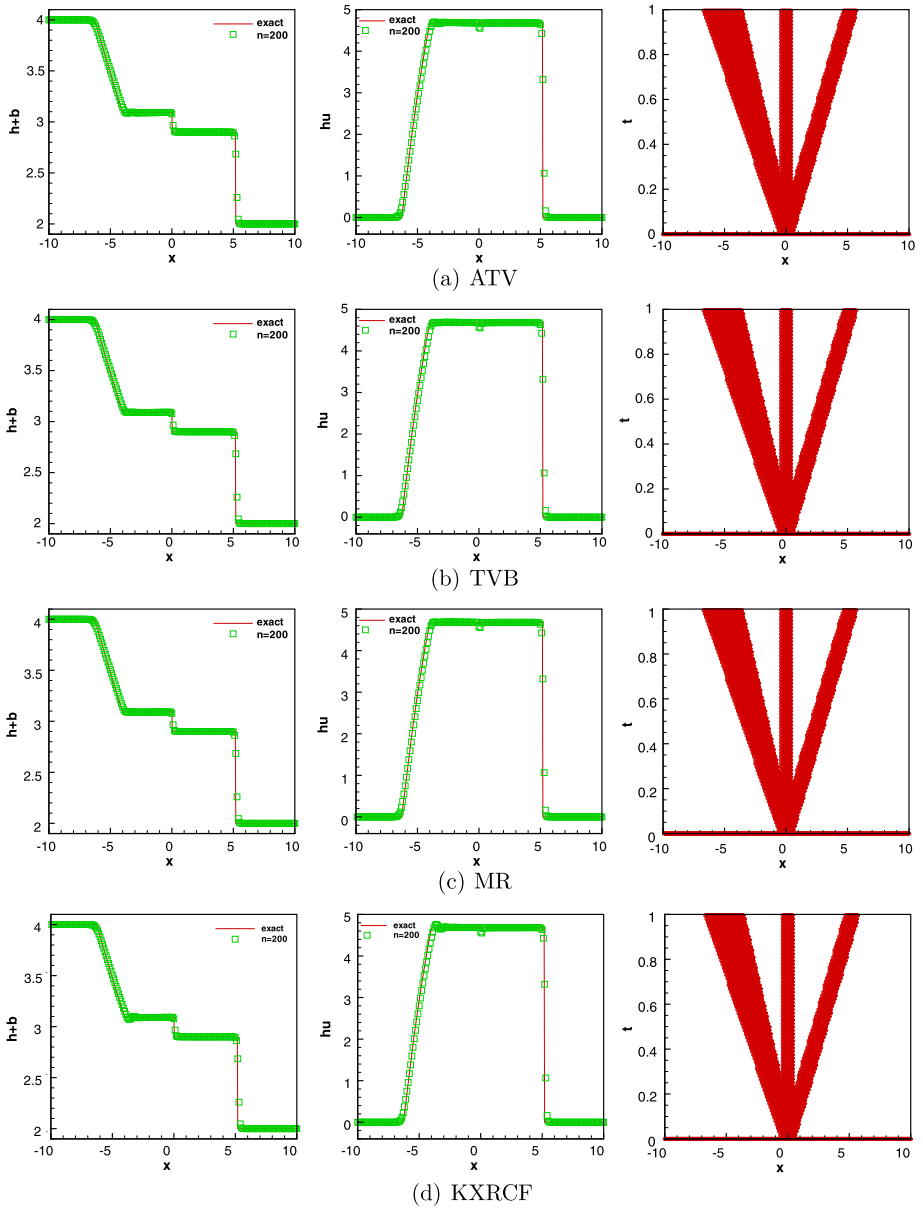

Fig. 3 1-rarefaction and 2-shock problem by the 5th-order scheme with different indicators, $t = 1$. From *left* to *right*: water surface level $h + b$, water discharge hu and time history of reconstruction of fluxes by WENO approximation

with mesh refinement in most cases, which is a very desirable property for the troubled-cell indicators. For all the indicators, we show the water surface level, the water discharge at $t = 1$ against the exact solution and time history of reconstruction of fluxes by WENO approximation in Fig. 4. It is evident that the numerical results for all cases have a good

Table 4 1-shock and 2-shock problem. Comparison on CPU time and percentage of reconstruction of fluxes by WENO approximation among original well-balanced WENO and hybrid well-balanced WENO schemes

N	Scheme or indicators	3rd-order		5th-order		7th-order		9th-order	
		CPU	Percent	CPU	Percent	CPU	Percent	CPU	Percent
50	WENO	0.09	100.00	0.11	100.00	0.16	100.00	0.25	100.00
	ATV	0.05	33.03	0.06	31.41	0.08	42.23	0.13	46.95
	TVB	0.06	52.41	0.06	50.75	0.09	52.60	0.14	55.24
	MR	0.06	41.40	0.05	40.16	0.09	48.42	0.11	52.64
	KXRCF	0.06	17.72	0.05	17.91	0.05	17.94	0.08	17.98
100	WENO	0.36	100.00	0.34	100.00	0.55	100.00	0.92	100.00
	ATV	0.13	21.66	0.11	20.78	0.22	27.44	0.34	30.26
	TVB	0.16	36.67	0.17	39.87	0.28	40.68	0.44	41.88
	MR	0.11	29.11	0.16	29.71	0.25	35.49	0.41	40.46
	KXRCF	0.13	9.84	0.15	11.42	0.16	12.68	0.17	13.29
200	WENO	1.23	100.00	1.30	100.00	2.14	100.00	3.77	100.00
	ATV	0.34	13.37	0.34	12.32	0.58	17.91	0.97	20.59
	TVB	0.45	23.26	0.53	33.04	0.91	33.69	1.39	34.29
	MR	0.41	18.59	0.45	23.92	0.88	30.51	1.39	33.56
	KXRCF	0.34	10.54	0.36	11.74	0.50	12.70	0.72	13.21

resolution and are mostly free of oscillations. Due to the space limitation, we only present the numerical results of the 5th-order schemes.

3.4 A Small Perturbation of a Steady-state Water

The following quasi-stationary test was proposed by LeVeque [10]. It was chosen to demonstrate the capability of the hybrid well-balanced WENO scheme for the computation on a rapidly varying flow over a smooth bottom, and the perturbation of a stationary state. The bottom topography consists of a bump

$$b(x) = \begin{cases} 0.25(\cos(10\pi(x-1.5))+1) & \text{if } 1.4 \le x \le 1.6, \\ 0 & \text{otherwise,} \end{cases}$$

the initial condition are given as

$$h(x,0) = \begin{cases} 1-b(x)+\epsilon & \text{if } 1.1 \le x \le 1.2, \\ 1-b(x) & \text{otherwise,} \end{cases} \quad \text{and} \quad u(x,0) = 0,$$

where ϵ is a non-zero perturbation constant. Two cases have been run: $\epsilon = 0.2$ (big pulse) and $\epsilon = 0.001$ (small pulse).

We present the CPU time and the percentages of reconstruction of fluxes by WENO approximation for the two cases in Tables 5 and 6, respectively. Table 5 of big pulse shows that the hybrid schemes can save the computational cost by about 50% and only about 30–50% reconstruction of fluxes are approximated by WENO approximation. Table 6 of small

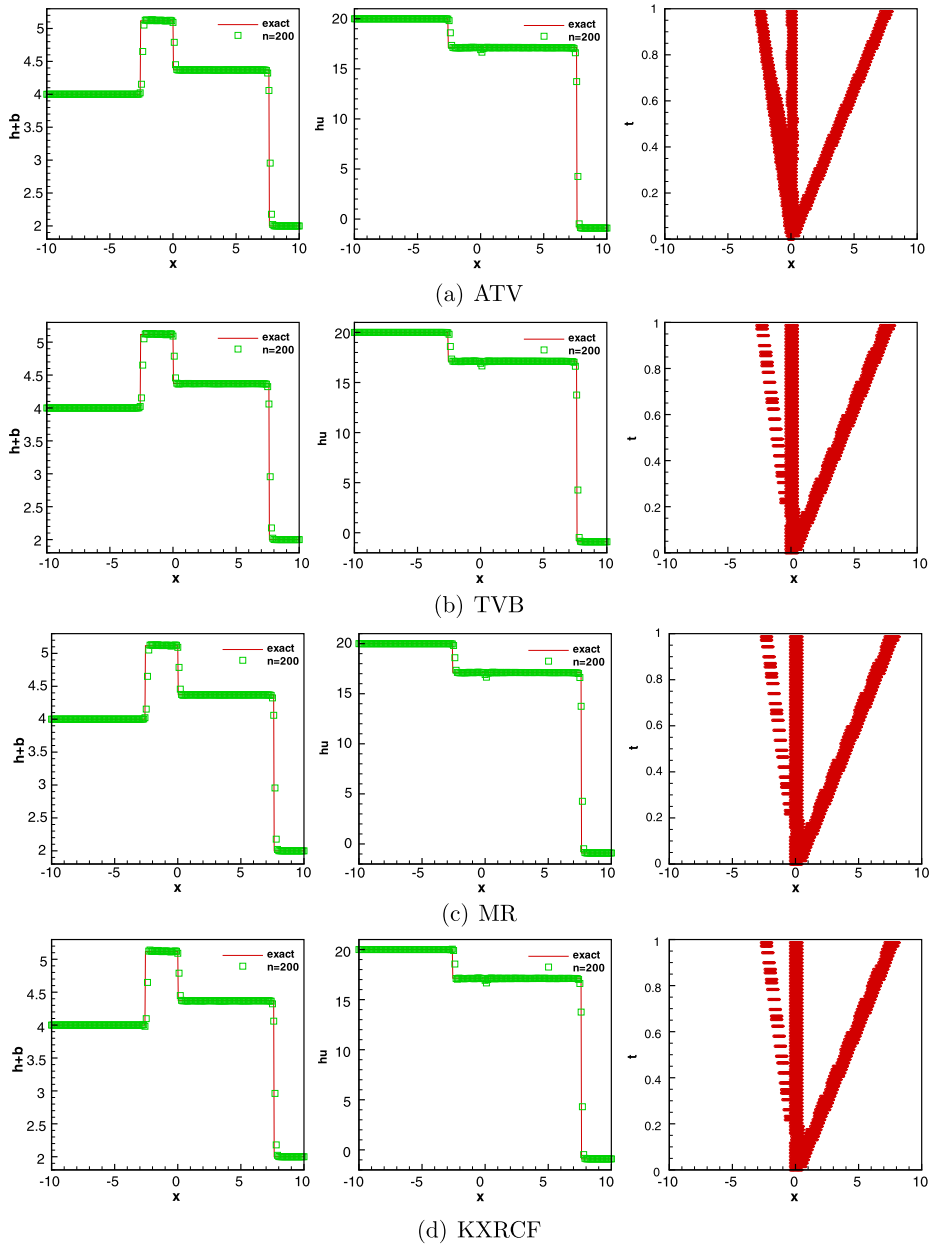

Fig. 4 1-shock and 2-shock problem by the 5th-order scheme with different indicators, 200 cells, $t = 1$. From *left* to *right*: water surface level $h + b$, water discharge hu and time history of reconstruction of fluxes by WENO approximation

pulse shows that the hybrid schemes can save the computational cost by about 45% and only about 30% reconstruction of fluxes are approximated by WENO approximation. We can observe that the percentages of reconstruction of fluxes by WENO approximation decrease

Table 5 Small perturbation of a steady-state with a big pulse. Comparison on CPU time and percentage of reconstruction of fluxes by WENO approximation among original well-balanced WENO and hybrid well-balanced WENO schemes

N	Scheme or indicators	3rd-order		5th-order		7th-order		9th-order	
		CPU	Percent	CPU	Percent	CPU	Percent	CPU	Percent
50	WENO	0.08	100.00	0.11	100.00	0.13	100.00	0.16	100.00
	ATV	0.03	52.63	0.05	54.13	0.08	58.35	0.11	63.81
	TVB	0.05	72.30	0.05	73.50	0.08	74.93	0.13	76.47
	MR	0.05	51.84	0.05	56.03	0.09	63.93	0.11	69.04
	KXRCF	0.06	67.95	0.05	71.64	0.08	72.31	0.11	74.63
100	WENO	0.23	100.00	0.23	100.00	0.36	100.00	0.66	100.00
	ATV	0.11	39.94	0.11	40.59	0.20	43.14	0.32	46.08
	TVB	0.14	56.56	0.19	61.09	0.27	62.72	0.44	63.61
	MR	0.08	37.00	0.11	40.55	0.20	43.89	0.33	46.82
	KXRCF	0.13	49.19	0.12	65.56	0.23	55.57	0.38	57.59
200	WENO	0.88	100.00	0.95	100.00	1.44	100.00	2.42	100.00
	ATV	0.34	31.91	0.39	32.00	0.59	33.30	0.97	34.79
	TVB	0.42	41.02	0.52	45.68	0.75	46.78	1.34	51.22
	MR	0.31	24.42	0.38	27.15	0.50	29.73	0.84	32.28
	KXRCF	0.36	31.65	0.40	50.29	0.61	35.89	1.06	38.89

Table 6 Small perturbation of a steady-state with a small pulse. Comparison on CPU time and percentage of reconstruction of fluxes by WENO approximation among original well-balanced WENO and hybrid well-balanced WENO schemes

N	Scheme or indicators	3rd-order		5th-order		7th-order		9th-order	
		CPU	Percent	CPU	Percent	CPU	Percent	CPU	Percent
50	WENO	0.07	100.00	0.08	100.00	0.09	100.00	0.14	100.00
	ATV	0.05	51.45	0.05	53.01	0.08	57.27	0.09	62.75
	TVB	0.03	49.49	0.05	57.54	0.06	62.81	0.11	67.68
	MR	0.03	25.22	0.03	41.18	0.06	51.99	0.09	59.77
	KXRCF	0.05	61.39	0.05	66.40	0.06	69.57	0.11	71.40
100	WENO	0.20	100.00	0.22	100.00	0.34	100.00	0.59	100.00
	ATV	0.11	38.97	0.12	39.23	0.16	42.08	0.31	44.66
	TVB	0.11	39.27	0.13	45.72	0.19	47.88	0.28	50.26
	MR	0.09	32.49	0.11	38.55	0.19	42.05	0.31	45.00
	KXRCF	0.13	42.78	0.12	43.99	0.22	47.29	0.36	50.27
200	WENO	0.70	100.00	0.73	100.00	1.38	100.00	2.16	100.00
	ATV	0.33	30.85	0.32	30.71	0.56	31.82	0.83	33.26
	TVB	0.30	26.62	0.31	32.95	0.67	36.28	1.02	37.86
	MR	0.32	30.18	0.33	31.08	0.58	32.30	0.91	33.82
	KXRCF	0.31	30.19	0.31	32.59	0.64	34.13	0.95	35.86

with mesh refinement in most cases, which is a very desirable property for troubled-cell indicators. For all the indicators, we show the water surface level, the water discharge at $t = 0.2$ against the reference solution and time history of reconstruction of fluxes by WENO approximation in Fig. 5 (big pulse) and Fig. 6 (small pulse). In the water surface level and the water discharge figures, the solid line is the reference solution computed by the 5th-order finite difference WENO scheme using 3000 grid points. The numerical results are resolved accurately, free of spurious numerical oscillations, and look very comparable to those found in the other existing literature. In order to save space, in this paper we do not present the results by the 3rd-, 7th- and 9th-order schemes which are similar to those by the 5th-order scheme.

3.5 The Dam Break Problem over a Rectangular Bump

In this example, we simulate a dam break problem over a rectangular bump, which involves a rapidly varying flow over a discontinuous bottom. The computational domain is [0, 1500]. The bottom topography has the following form

$$b(x) = \begin{cases} 8 & \text{if } |x - 750| \le 1500/8, \\ 0 & \text{otherwise}, \end{cases}$$

the initial conditions are given by

$$h(x,0) = \begin{cases} 20 - b(x) & \text{if } x \le 750, \\ 15 - b(x) & \text{otherwise}, \end{cases} \quad \text{and} \quad u(x,0) = 0.$$

In Table 7, we compare the CPU time and the percentages of reconstruction of fluxes by WENO approximation between the original well-balanced WENO schemes and the hybrid well-balanced WENO schemes. Table 7 indicates that the hybrid schemes can save the computational cost by about 80% and only about 20–30% reconstruction of fluxes are approximated by WENO approximation. We can observe that the percentages of reconstruction of fluxes by WENO approximation decrease with mesh refinement in most cases. For all the indicators, we show the water surface level, the water discharge at $t = 15$ against the reference solution and time history of reconstruction of fluxes by WENO approximation in Fig. 7. In the water surface level and the water discharge figures, the solid line is the reference solution computed by the 5th-order finite difference WENO scheme using 3000 grid points. It is clear that the numerical results are resolved accurately and almost free of oscillations. In order to save space, we only present the numerical results of the 5th-order schemes, for the results by the 3rd-, 7th- and 9th-order schemes which are similar to those by the 5th-order schemes.

3.6 A Small Perturbation of a Two-dimensional Steady-state Water

This is a classical example to show the capability of the proposed scheme for the perturbation of the stationary state, given by LeVeque [10]. The PDEs are (2.10). We solve the system in a rectangular domain $[0, 2] \times [0, 1]$. The bottom topography is an isolated elliptical shaped hump

$$b(x, y) = 0.8e^{-5(x-0.9)^2-50(y-0.5)^2},$$

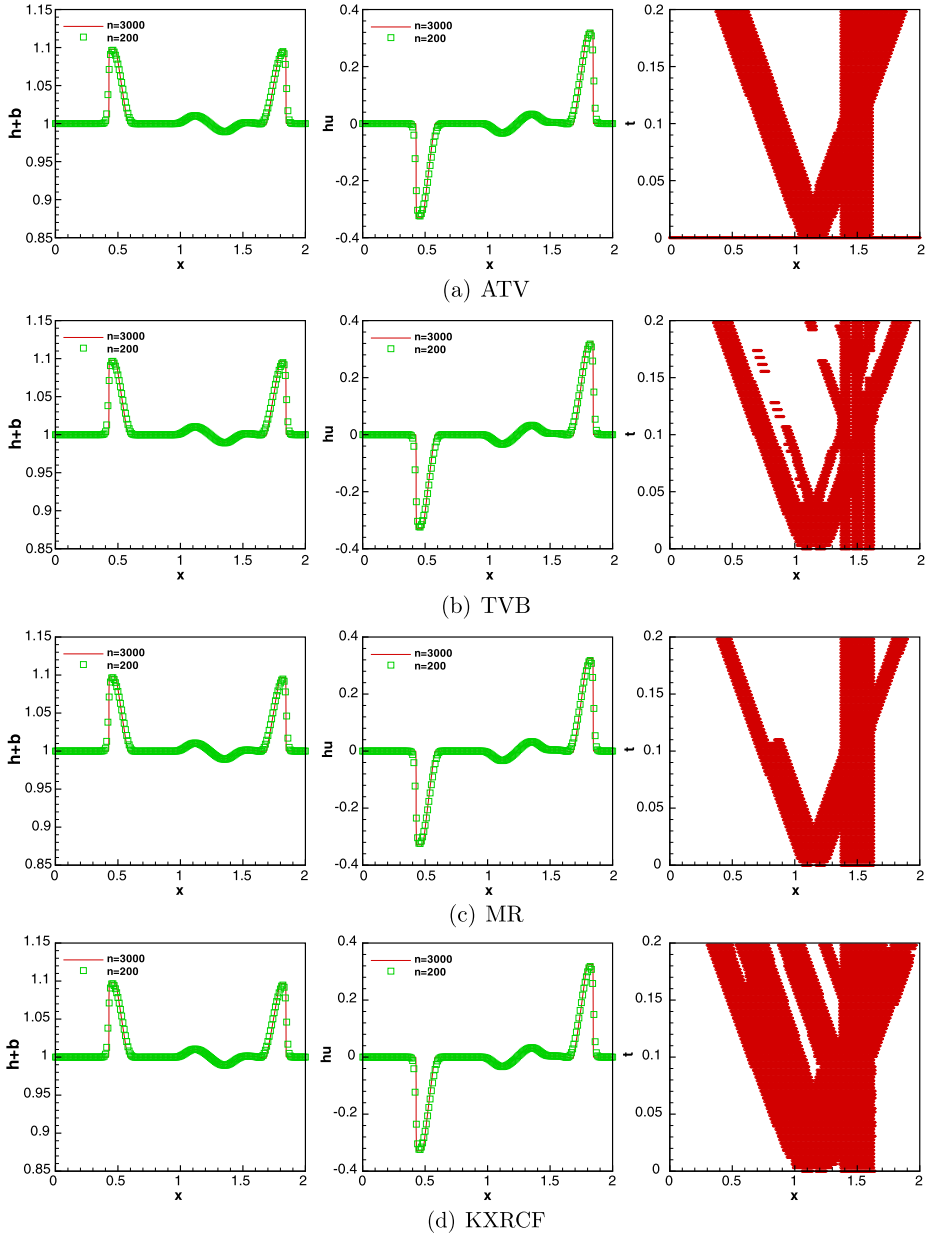

Fig. 5 Small perturbation of a steady-state with a big pulse by the 5th-order scheme with different indicators, 200 cells, $t = 0.2$. From *left* to *right*: water surface level $h + b$, water discharge hu and time history of reconstruction of fluxes by WENO approximation

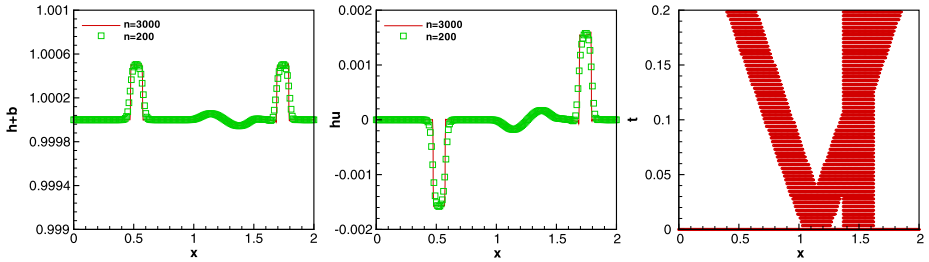

(a) ATV

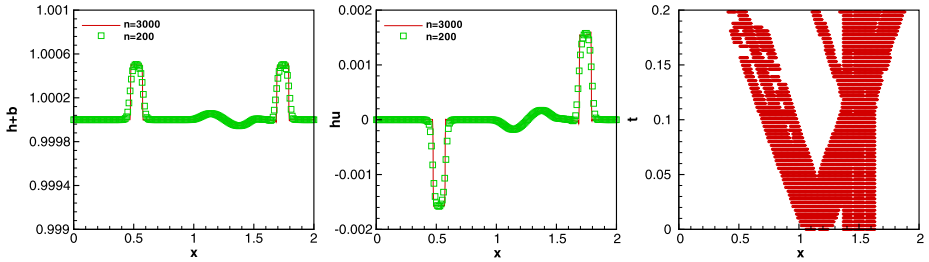

(b) TVB

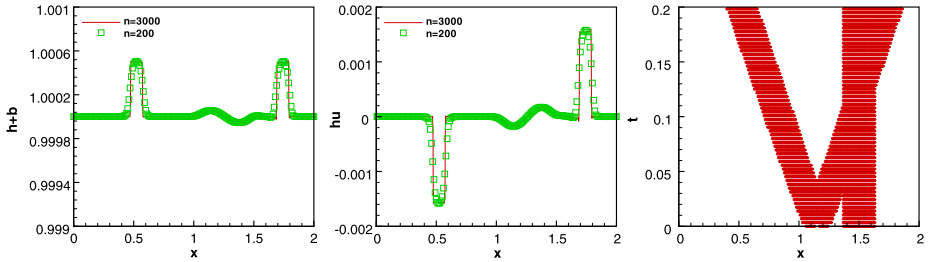

(c) MR

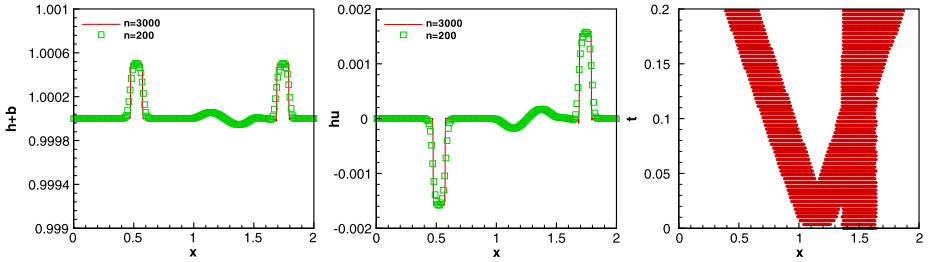

(d) KXRCF

Fig. 6 Small perturbation of a steady-state with a small pulse by the 5th-order scheme with different indicators, 200 cells, $t = 0.2$. From *left* to *right*: water surface level $h + b$, water discharge hu and time history of reconstruction of fluxes by WENO approximation

Table 7 The dam break problem over a rectangular bump. Comparison on CPU time and percentage of reconstruction of fluxes by WENO approximation among original well-balanced WENO and hybrid well-balanced WENO schemes

N	Scheme or indicators	3rd-order		5th-order		7th-order		9th-order	
		CPU	Percent	CPU	Percent	CPU	Percent	CPU	Percent
50	WENO	0.04	100.00	0.05	100.00	0.06	100.00	0.07	100.00
	ATV	0.02	40.42	0.03	43.89	0.04	47.66	0.05	51.28
	TVB	0.01	31.57	0.02	35.59	0.03	39.82	0.04	42.34
	MR	0.02	25.34	0.02	32.88	0.03	40.12	0.03	47.36
	KXRCF	0.03	76.47	0.03	80.24	0.04	82.17	0.05	84.74
100	WENO	0.09	100.00	0.08	100.00	0.16	100.00	0.23	100.00
	ATV	0.05	29.06	0.05	32.25	0.06	35.26	0.09	37.85
	TVB	0.02	11.88	0.05	15.84	0.06	19.80	0.08	23.76
	MR	0.03	15.23	0.03	23.27	0.07	27.99	0.09	31.98
	KXRCF	0.05	42.42	0.06	50.88	0.09	48.48	0.18	70.98
200	WENO	0.34	100.00	0.36	100.00	0.58	100.00	0.89	100.00
	ATV	0.09	19.45	0.11	20.98	0.19	33.30	0.28	25.67
	TVB	0.08	6.08	0.09	8.45	0.11	46.78	0.16	13.91
	MR	0.09	12.04	0.09	16.04	0.18	29.73	0.25	23.12
	KXRCF	0.13	23.08	0.14	26.69	0.17	35.89	0.36	33.45

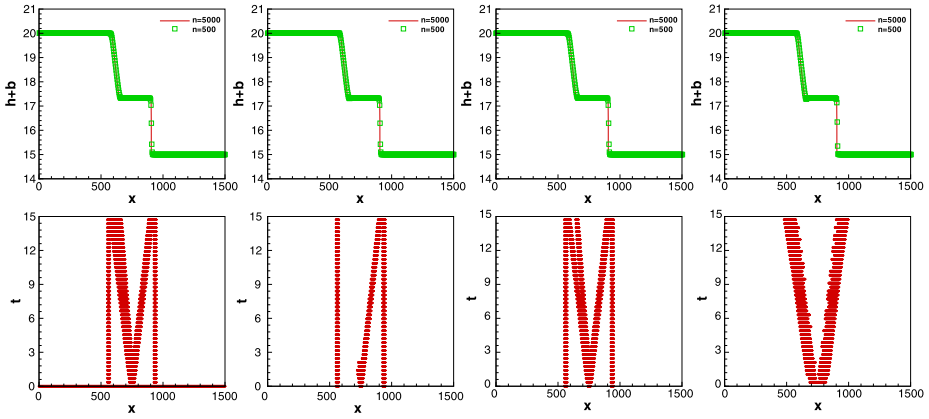

Fig. 7 The dam break problem over a rectangular bump by the 5th-order with different indicators, 500 cells, $t = 15$. Water surface level $h + b$ (*top*) and time history of reconstruction of fluxes by WENO approximation (*bottom*). From left to right: ATV, TVB, MR and KXRCF

the initial conditions are given by

$$h(x, y, 0) = \begin{cases} 1 - b(x, y) + 0.01 & \text{if } 0.05 \le x \le 0.15, \\ 1 - b(x, y) & \text{otherwise,} \end{cases} \quad \text{and} \quad u(x, y, 0) = v(x, y, 0) = 0.$$

Table 8 A small perturbation of a two-dimensional steady-state water, $t = 0.24$. Comparison on CPU time and percentage of reconstruction of fluxes by WENO approximation among the original well-balanced WENO and the hybrid well-balanced WENO schemes

$N_x \times N_y$	Scheme or indicators	3rd-order		5th-order	
		CPU	Percent	CPU	Percent
150×75	WENO	5.95	100.00	9.84	100.00
	ATV	2.07	8.52	2.13	8.36
	TVB	2.31	7.84	2.57	10.68
	MR	2.06	7.64	2.09	7.31
	KXRCF	2.55	8.49	2.83	10.51
300×150	WENO	47.81	100.00	78.66	100.00
	ATV	14.25	5.88	15.82	5.65
	TVB	18.25	5.25	19.45	7.93
	MR	15.47	6.14	16.21	5.97
	KXRCF	19.81	4.41	20.57	6.46
600×300	WENO	408.07	100.00	637.23	100.00
	ATV	103.79	3.05	131.20	3.40
	TVB	112.14	4.25	161.91	5.91
	MR	127.35	4.97	139.12	4.81
	KXRCF	111.22	2.10	166.87	3.89

Table 9 A small perturbation of a two-dimensional steady-state water, $t = 0.48$. Comparison on CPU time and percentage of reconstruction of fluxes by WENO approximation among the original well-balanced WENO and the hybrid well-balanced WENO schemes

$N_x \times N_y$	Scheme or indicators	3rd-order		5th-order	
		CPU	Percent	CPU	Percent
150×75	WENO	11.92	100.00	19.77	100.00
	ATV	4.17	11.57	4.47	11.61
	TVB	4.62	9.62	5.41	14.17
	MR	4.09	6.85	4.24	8.58
	KXRCF	5.05	7.64	5.87	13.93
300×150	WENO	95.65	100.00	156.47	100.00
	ATV	31.42	8.00	32.95	7.96
	TVB	33.66	6.24	39.75	10.55
	MR	31.34	7.20	33.24	7.72
	KXRCF	38.97	3.18	41.81	7.65
600×300	WENO	815.73	100.00	1274.02	100.00
	ATV	253.64	5.18	270.07	4.98
	TVB	298.85	4.71	328.71	7.90
	MR	256.00	6.54	287.09	6.70
	KXRCF	301.59	1.37	334.37	4.12

In Tables 8–9, we document the CPU time and the percentages of reconstruction of fluxes by WENO approximation by the 3rd- and the 5th-order schemes at $t = 0.24$ and $t = 0.48$, respectively. We can clearly see that the hybrid well-balanced WENO schemes can save 60–75% computational cost compared with the original well-balanced WENO schemes and only less 15% reconstruction of fluxes are approximated by WENO approxi-

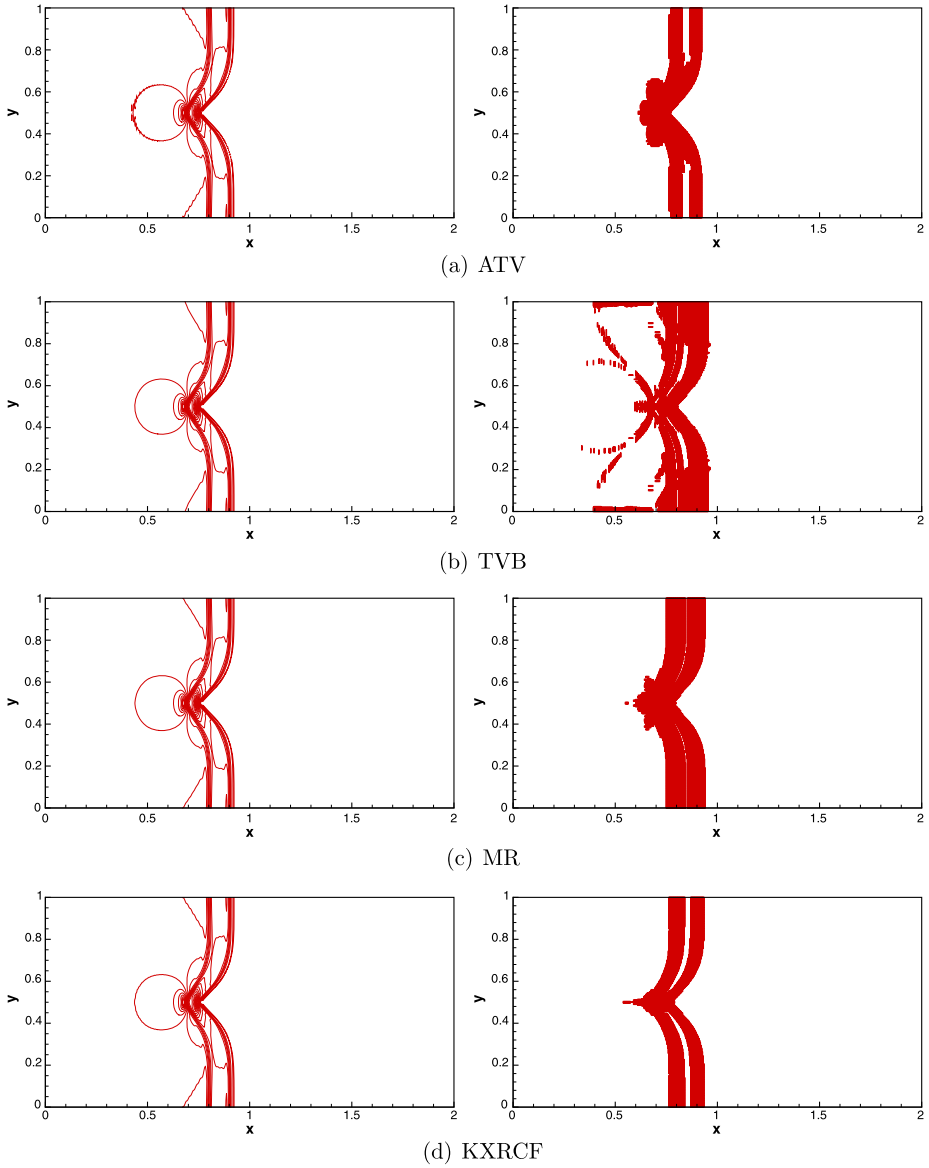

Fig. 8 A small perturbation of a two-dimensional steady-state water by the 5th-order schemes with different indicators, 600×300 cells, $t = 0.24$. Contours of $h + b$ (*left*) and reconstructions of fluxes by WENO approximation at the last time step (*right*)

mation. It is desirable that smaller percentage of reconstruction of fluxes are approximated by WENO approximation with finer meshes. To save space, we only show the contours of the water surface level $h + b$ and reconstructions of fluxes by WENO approximation at the last time step on the most refined mesh with 600×300 uniform cells by the 5th-order schemes at $t = 0.24$ and $t = 0.48$ in Figs. 8 and 9, respectively. Figures 8 and 9

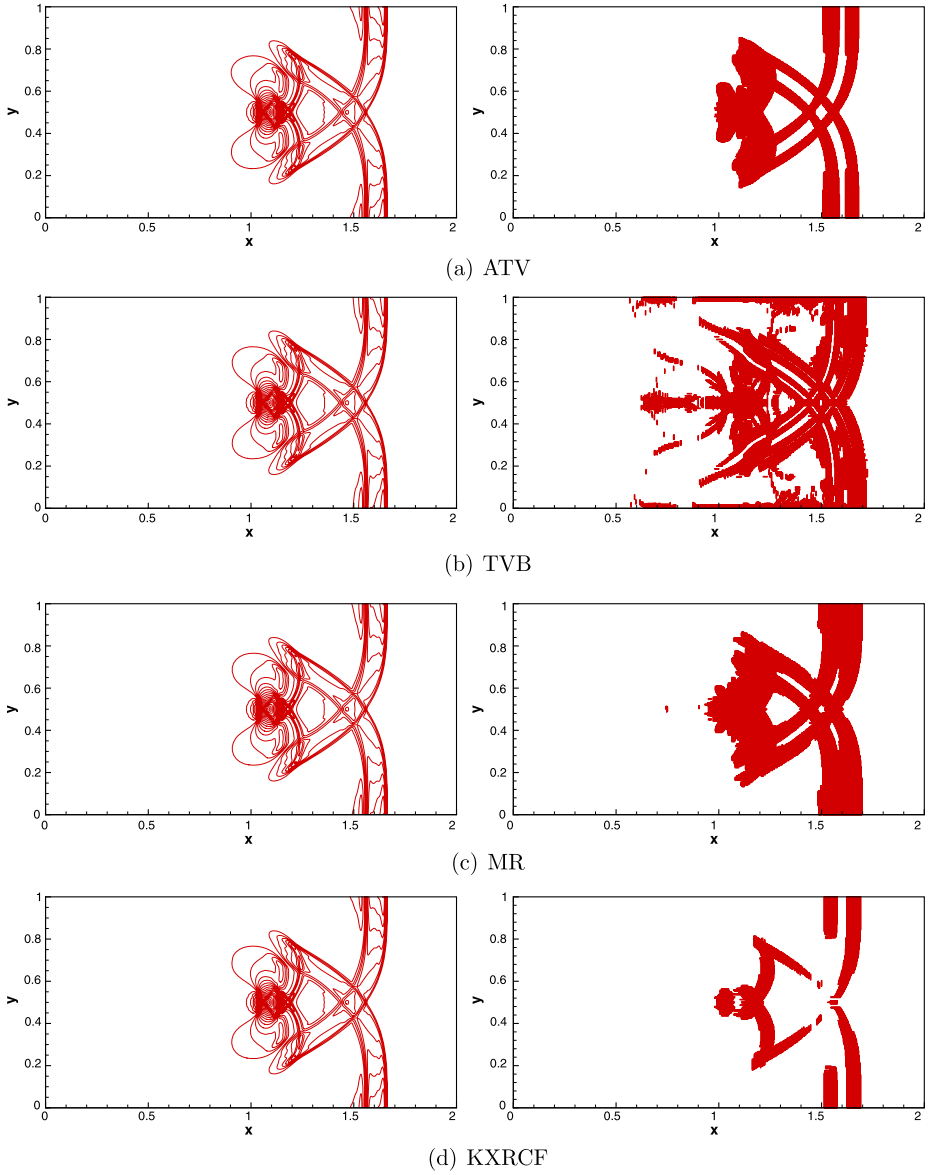

Fig. 9 A small perturbation of a two-dimensional steady-state water by the 5th-order schemes with different indicators, 600×300 cells, $t = 0.48$. Contours of $h + b$ (*left*) and reconstructions of fluxes by WENO approximation at the last time step (*right*)

display the right-going disturbance as it propagates past the hump. The numerical results suggest that our schemes can resolve the complex small-scale features of the flow very well.

Table 10 Two-dimensional dam break problem. Comparison on CPU time and percentage of reconstruction of fluxes by WENO approximation among original WENO and hybrid WENO schemes

$N_x \times N_y$	Scheme or indicators	3rd-order		5th-order	
		CPU	Percent	CPU	Percent
100×100	WENO	1.72	100.00	3.05	100.00
	ATV	0.60	25.08	0.76	37.47
	TVB	0.50	2.90	0.58	11.61
	MR	0.46	1.65	0.52	5.69
	KXRCF	0.54	3.07	0.67	6.03
200×200	WENO	22.63	100.00	39.66	100.00
	ATV	7.35	8.00	9.16	29.31
	TVB	4.50	6.24	5.04	10.55
	MR	5.99	7.20	6.83	4.39
	KXRCF	6.95	4.18	7.25	5.36
400×400	WENO	308.82	100.00	546.95	100.00
	ATV	106.91	14.64	161.00	14.19
	TVB	99.36	2.37	144.42	4.72
	MR	92.40	2.34	138.48	3.68
	KXRCF	103.12	2.13	147.28	4.15

3.7 Two-dimensional Dam Break Problem

This two-dimensional dam break problem is the one presented in [6]. The numerical example deals with a partial failure of a dam. The objective of this test case is to study the capability of the scheme. We consider the test case of a partial dam break on a flat bottom ($b = 0$) and the computational domain is a square domain $[0, 200] \times [0, 200]$, where the water flows from left to right through a breach located at $x = 100$, between $y = 95$ and $y = 170$. The initial water depth and velocity are as follows

$$h(x, y, 0) = \begin{cases} 10 & \text{if } x \leq 100, \\ 5 & \text{otherwise,} \end{cases} \quad \text{and} \quad u(x, y, 0) = v(x, y, 0) = 0.$$

The boundary conditions at $x = 0$ and $x = 200$ are assumed to be transmissive and all the others are imposed with reflective boundary conditions. We solve this problem up to $t = 7.2$.

In Table 10, we document the CPU time and the percentages of reconstruction of fluxes by WENO approximation. We can obviously observe that the hybrid well-balanced WENO schemes can save 65–75% computational cost compared with the original well-balanced WENO schemes and only less 40% reconstruction of fluxes are approximated by WENO approximation. It is evident that the smaller percentage of reconstruction of fluxes are approximated by WENO approximation with the finer meshes as we expect. To save space, we only show the numerical results on the most refined mesh with 400×400 uniform cells by the 5th-order scheme at $t = 0.72$ in Fig. 10. The numerical results indicate that the schemes provide a very high resolution of both the circular shock wave and the vortices formed on the breach. Reconstructions of fluxes by WENO approximation at the last time step are shown in Fig. 11.

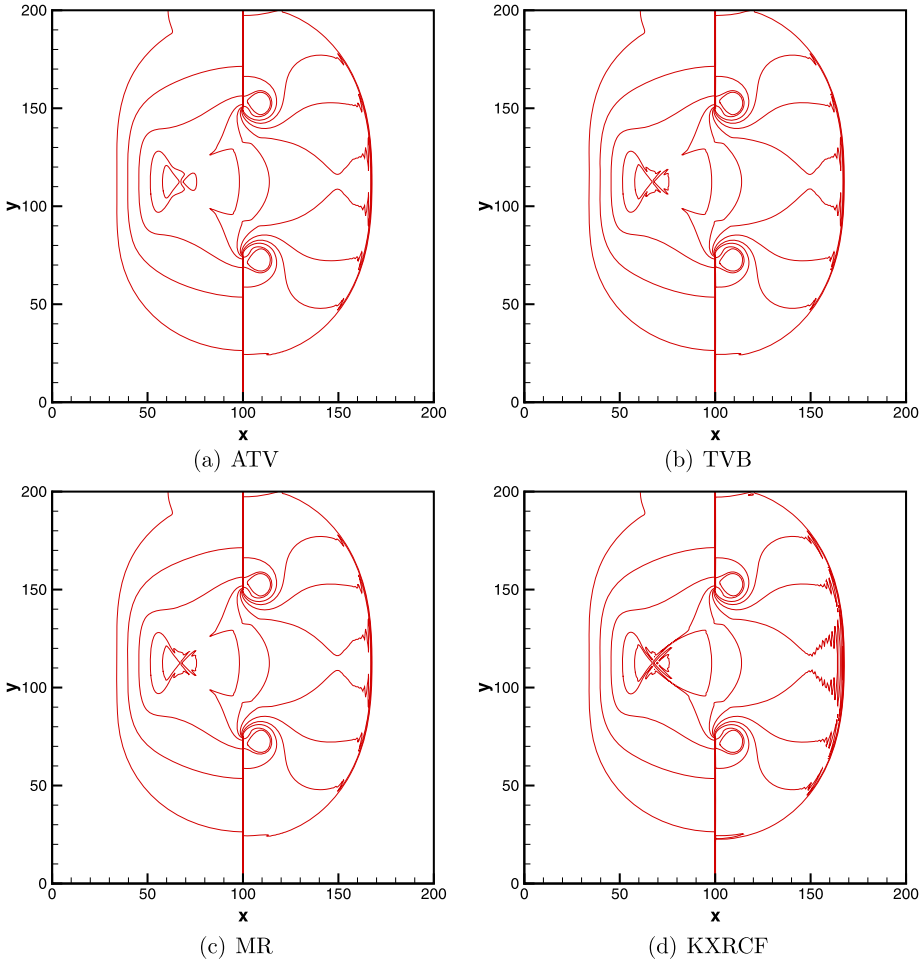

Fig. 10 Two-dimensional dam break problem by hybrid well-balanced WENO schemes with different indicators, 400×400 cells, $t = 7.2$. Water depth contours

4 Concluding Remarks

In this paper, we continue studying the hybridization of the WENO schemes with the high order up-wind linear schemes in [11] to solve the shallow water equations on non-flat bottom topography. Extensive numerical results of one- and two-dimensional cases indicate that the hybrid well-balanced WENO schemes have the following properties: good capturing of the strong discontinuities, high resolution, essentially non-oscillatory and sharp shock transition and saving computational cost.

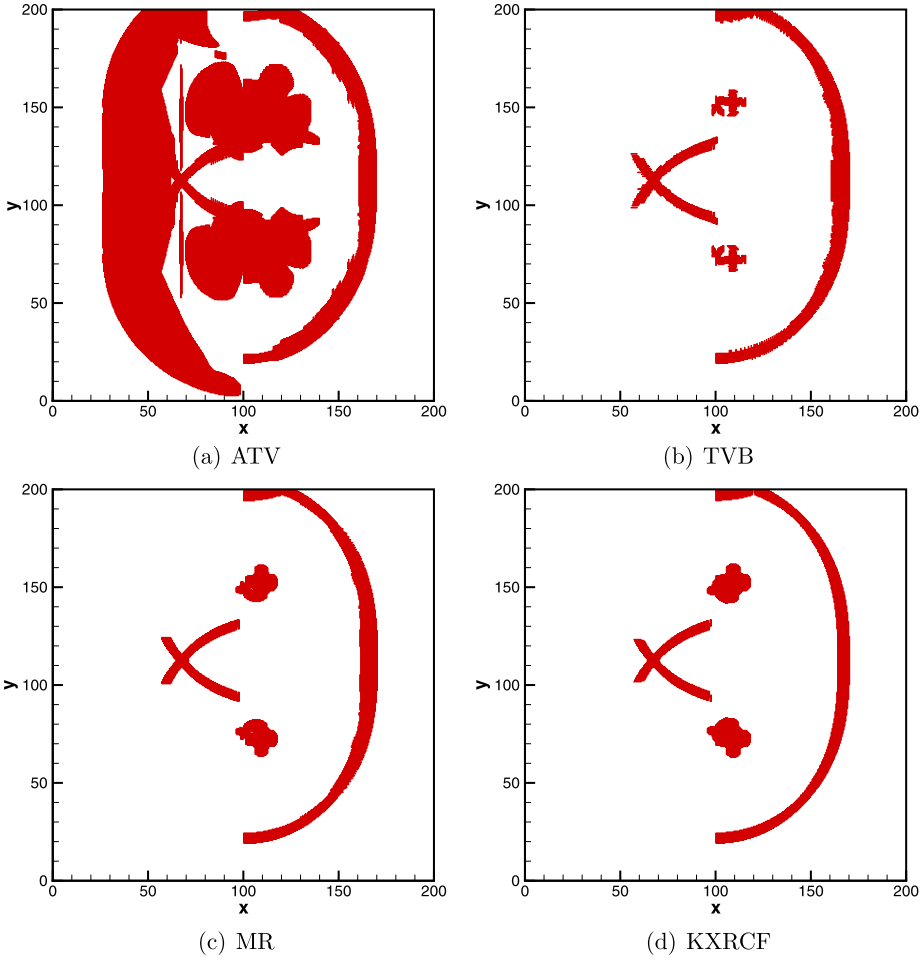

Fig. 11 Two-dimensional dam break problem by hybrid well-balanced WENO schemes with different indicators, 400×400 cells, $t = 7.2$. Reconstructions of fluxes by WENO approximation at the last time step

References

1. Alcrudo, F., Benkhaldoun, F.: Exact solution to the Riemann problem of the shallow water euqaionts with a bottom step. Comput. Fluids **30**, 643–671 (2001)
2. Bermudez, A., Vazquez, M.E.: Upwind methods for hyperbolic conservation laws with source terms. Comput. Fluids **23**, 1049–1071 (1994)
3. Cockburn, B., Shu, C.-W.: TVB Runge-Kutta local projection discontinuous Galerkin finite element method for conservation laws II: General framework. Math. Comput. **52**, 411–435 (1989)
4. Cosat, B., Don, W.S.: High order hybrid central-WENO finite difference scheme for conservation laws. J. Comput. Appl. Math. **204**, 209–218 (2007)
5. Crnjaric, N., Vukovic, S., Sopta, L.: Extension of ENO and WENO schemes to one-dimensional sediment transport equations. Comput. Fluids **33**, 31–56 (2004)
6. Fennema, R.J., Chaudhry, M.H.: Explicit methods for 2D transient free surface flows. J. Hydraul. Eng. **116**, 1013–1034 (1990)
7. Harten, A.: Adaptive multiresolution schemes for shock computations. J. Comput. Phys. **115**, 319–338 (1994)

8. Jiang, G., Shu, C.-W.: Efficient implementation of weighted ENO schemes. J. Comput. Phys. **126**, 202–228 (1996)
9. Krivodonova, L., Xin, J., Remacle, J.-F., Chevaugeon, N., Flaherty, J.: Shock detection and limiting with discontinuous Galerkin methods for hyperbolic conservation laws. Appl. Numer. Math. **48**, 323–338 (2004)
10. LeVeque, R.J.: Balancing source terms and flux gradient on high-resolution Godunov methods: the quasi-steady wave-propagation algorithm. J. Comput. Phys. **146**, 346–365 (1998)
11. Li, G., Qiu, J.: Hybrid weighted essentially non-oscillatory schemes with different indicators. J. Comput. Phys. **229**, 8105–8129 (2010)
12. Pirozzoli, S.: Conservative hybrid compact-WENO schemes for shock-turbulence interaction. J. Comput. Phys. **178**, 81–117 (2002)
13. Qiu, J., Shu, C.-W.: A comparison of troubled-cell indicators for Runge-Kutta discontinuous Galerkin methods using weighted essentially nonoscillatory limiters. SIAM J. Sci. Comput. **27**, 995–1013 (2005)
14. Rogers, B.D., Borthwick, A.G.L., Taylor, P.H.: Mathematical balancing of flux gradient and source terms prior to using Roe's approximate Riemann solver. J. Comput. Phys. **192**, 422–451 (2003)
15. Shu, C.-W., Osher, S.: Efficient implementiation of essentially non-oscillatory shock-capturing schemes. J. Comput. Phys. **77**, 439–471 (1988)
16. Shu, C.-W.: Essentially non-oscillatory and weighted essentially non-oscillatory schemes for hyperbolic conservation laws. NASA/CR-97-206253, ICASE Report NO.97-65 (1997)
17. Shu, C.-W.: High order weighted essentially nonoscillatory schemes for convection dominated problems. SIAM Rev. **51**, 82–126 (2009)
18. Toro, E.F.: Shock-capturing Methods for Free-surface Shallow Flows. Wiley, New York (2001)
19. Vukovic, S., Sopta, L.: ENO and WENO schemes with the exact conservation property for one-dimensional shallow water equations. J. Comput. Phys. **179**, 593–621 (2002)
20. Xing, Y., Shu, C.-W.: High order finite difference WENO schemes with the exact conservation property for the shallow water equations. J. Comput. Phys. **208**, 206–227 (2005)
21. Xing, Y., Shu, C.-W.: High-order well-balanced finite difference WENO schemes for a class of hyperbolic systems with source terms. J. Sci. Comput. **27**, 477–494 (2006)
22. Xing, Y., Shu, C.-W.: High order well-balanced finite volume WENO schemes and discontinuous Galerkin methods for a class of hyperbolic systems with source terms. J. Comput. Phys. **214**, 567–598 (2006)
23. Xing, Y., Zhang, X., Shu, C.-W.: Positivity-preserving high order well-balanced discontinuous Galerkin methods for the shallow water equations. Adv. Water Resour. **33**, 1476–1493 (2010)
24. Zhou, J.G., Causon, D.M., Mingham, C.G., Ingram, D.M.: The surface gradient method for the treatment of source terms in the shallow-water equations. J. Comput. Phys. **168**, 1–25 (2001)
25. Zhu, H., Qiu, J.: Adaptive Runge-Kutta discontinuous Galerkin methods using different indicators: one-dimensional case. J. Comput. Phys. **228**, 6957–6976 (2009)